

# Cost of Simulating Entanglement in Steering Scenario

Yujie Zhang<sup>1</sup>, Jiaxuan Zhang<sup>1</sup>, and Eric Chitambar<sup>2</sup>

<sup>1</sup>Department of Physics, University of Illinois at Urbana-Champaign, Urbana, IL 61801, USA

<sup>2</sup> Department of Electrical and Computer Engineering, University of Illinois at Urbana-Champaign, Urbana, IL 61801, USA

Quantum entanglement is a fundamental feature of quantum mechanics, yet certain entangled states that are unsteerable can be classically simulated in steering scenarios, making them unable to exhibit non-locality in quantum steering. Despite their significance, a systematic comparison of such entangled states has not been fully explored. In this work, we quantify the resource content of unsteerable quantum states in terms of the amount of shared randomness required to simulate their dynamical behavior in the steering scenario. We rigorously demonstrate that the simulation cost is unbounded even for some two-qubit unsteerable states. Moreover, the simulation cost of entangled two-qubit states is always strictly greater than that for any separable state.

A significant portion of our results rely on the relationship between the simulation cost of two-qubit Werner states and that of noisy spin measurements. Using noisy spin measurements as a central example, we investigate the minimal number of outcomes required for a parent measurement to simulate a given set of compatible measurements. Although some continuous sets of measurements can be simulated using a finite-outcome parent, we identify scenarios where the simulation cost diverges. Our results provide previously unknown lower bounds on the simulation cost, supported by connections between the simulation cost of noisy spin measurements and various geometric inequalities, including those studied in the zonotope-approximation problem in Banach space theory.

## 1 Introduction

In quantum information theory, entanglement is recognized as a resource because it enables certain dynamical processes (i.e. channels) that would otherwise be impossible, or at least more costly, to perform. For instance, shared entanglement can be used in conjunction with some noisy classical channel to increase its zero-error transmission [1, 2]. Another dramatic effect is quantum teleportation, in which a

Yujie Zhang: [yujie4physics@gmail.com](mailto:yujie4physics@gmail.com)

Eric Chitambar: [echitamb@illinois.edu](mailto:echitamb@illinois.edu)

classical channel is combined with shared entanglement to generate a perfect quantum channel [3]. In these examples, entanglement is used for the purpose of channel coding as it helps transform a noisy channel into a noiseless one. The converse task, analogous to the “Reverse Shannon” problem [4, 5], considers how much noiseless resource is needed to simulate a noisy entanglement-enhanced setup. Here the goal is not communication but rather simulation. From this perspective, one can quantify the resource value of an entangled state by how much classical resources are needed to simulate the dynamics that it generates.

Besides the standard entanglement-assisted paradigm, there are a variety of other ways in which a bipartite entangled state can be used to build a channel [6], and each of them will typically have a different simulation cost. In this letter, we focus on the type of channels that emerge in quantum steering setups [7]. These are classical-to-classical-quantum (c-to-cq) channels that are generated when Alice measures her half of the state  $\rho_{AB}$  in some chosen manner, thereby collapsing Bob’s system into one of many possible post-measurement states. From a fundamental perspective, these channels are vital to the study of quantum nonlocality [8]. But more practically they have important application in semi-device-independent entanglement witnessing [9] and operational games [10].

As shown in Fig. 2, each input  $x$  to the channel corresponds to a local measurement choice for Alice, which we collectively represent by a family of positive operator-measures (POVMs)  $\{M_{a|x}\}_{a,x}$ . She receives a classical output  $a$  while Bob jointly receives the (un-normalized) quantum output

$$\sigma_{a|x} = \text{Tr}_A[(M_{a|x} \otimes \mathbb{I})\rho_{AB}] \quad (1)$$

with probability  $p(a|x) = \text{Tr}[\sigma_{a|x}]$ . It is convenient to denote a c-to-cq channel by the set of labeled quantum

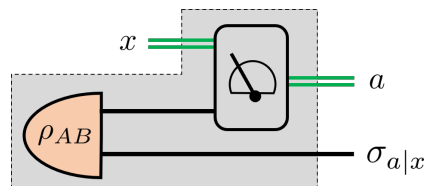


Figure 1: The bipartite state  $\rho_{AB}$  is transformed into a c-to-cq channel represented by the assemblage  $\mathcal{A} = \{\sigma_{a|x}\}$ .

outputs  $\mathcal{A} = \{\sigma_{a|x}\}$ , called a state assemblage [7], and we write  $\rho_{AB} \mapsto \mathcal{A}$  when Eq. (1) holds.

## 2 Preliminary

For a given quantum state  $\rho_{AB}$ , we wish to quantify the amount of classical resources needed to simulate each assemblage  $\mathcal{A}$  for which  $\rho_{AB} \mapsto \mathcal{A}$ . For this simulation task, it is natural to quantify the classical resource in terms of how much shared randomness Alice and Bob need to reproduce  $\mathcal{A}$  using a local hidden state (LHS) model. A LHS model for assemblage  $\mathcal{A} = \{\sigma_{a|x}\}$ , should it exist, is given by a shared random variable  $\lambda$  with distribution  $p(\lambda) > 0$ , a family of quantum states  $\{\rho_\lambda\}$  for Bob, and a classical channel  $p(a|x, \lambda)$  for Alice such that

$$\sigma_{a|x} = \sum_{\lambda \in \Lambda} p(a|x, \lambda) p(\lambda) \rho_\lambda \quad \forall \sigma_{a|x} \in \mathcal{A}. \quad (2)$$

Deploying this model requires Alice and Bob to have shared randomness of size  $|\Lambda| \in [1, +\infty]$ , and we define  $\gamma(\mathcal{A}) := \min |\Lambda|$  as the smallest possible cardinality of  $\Lambda$  for which Eq. (2) holds, and we refer to this as the *simulation cost* of state assemblage  $\mathcal{A}$ . For LHS models using a continuous shared variable, the sum in Eq. (2) is replaced with an integral, and thus the simulation cost will exist but remain unbounded.

If an assemblage  $\mathcal{A}$  does not admit a LHS model, then the resource transformation  $\rho_{AB} \mapsto \mathcal{A}$  constitutes the celebrated effect of quantum steering [8], specifically in the direction from Alice to Bob. Although entanglement is a necessary condition for steering, not all entangled states are steerable. For such states, the next natural question then is to look *beyond steering* and ask how much shared randomness is needed to simulate all the assemblages  $\mathcal{A}$  that the state can generate. For an unsteerable  $\rho_{AB}$ , we define  $\gamma(\rho_{AB}) := \max_{\mathcal{A}} \gamma(\mathcal{A})$  as the highest simulation cost to simulate any  $\mathcal{A}$  for which  $\rho_{AB} \mapsto \mathcal{A}$ .

We note that to be fully comprehensive, one should also consider the simulation cost  $\gamma(\mathcal{B})$  for any assemblage  $\mathcal{B}$  generated from  $\rho_{AB}$  by locally measuring on Bob's side since quantum steering is asymmetric between two parties [11, 12]. However, the specific examples we study in this work involve symmetric quantum states (under the exchange of parties). Consequently, our results remain general by just considering assemblages generated by local measurements on Alice's side. As an important special case that will be discussed in the paper, when Alice holds a qubit, we will also define  $\gamma^p(\rho_{AB}) := \max_{\mathcal{A}^p} \gamma(\mathcal{A}^p)$  as the simulation cost of simulating any  $\mathcal{A}^p$  generated by measurements that are confined to the  $x$ - $z$  plane, i.e.,  $M_{a|x}$  in Eq. (1) are all with Bloch vectors on the same ( $x$ - $z$ ) plane [13].

One important question we consider is whether the simulation cost  $\gamma(\rho_{AB})$  satisfies some general dimensionality bound. In fact, we always have  $\gamma(\rho_{AB}) \leq$

Singlet Weight	SR Cost $\gamma(\omega_r)$	State type
$r = 0$	$\gamma = 1$	product state
$0 < r \leq \frac{1}{3}$	$\gamma = 4$	separable
$\frac{1}{3} < r \leq \frac{1}{2}$	$\gamma > 4$ ; $\gamma = \Omega((\frac{1}{2} - r)^{-\frac{2}{3}})$	entangled and unsteerable
$\frac{1}{2} < r < 1$	—	steerable

Table 1: Simulation cost of two-qubit Werner-states  $\omega_r$ .

$(\dim(A))^2(\dim(B))^2$  for every separable state  $\rho_{AB}$  due the existence of minimal separable decompositions [14]. Does this bound also hold for unsteerable entangled states? This question was first raised and left unanswered by Brunner et al. in a study that established an upper bound on the simulation cost by explicitly constructing local hidden state models [15]. Later, Nguyen et al. proposed a geometric approach for characterizing quantum steering, which enables a more systematic search for upper bounds on the simulation cost of all two-qubit states under projective measurements [16]. Despite these advances, both works only provide upper bounds on  $\gamma(\rho_{AB})$ ; leaving open the possibility of better upper bound on the simulation models and preventing a direct resource comparison among entangled-unsteerable states.

In this work, we address the aforementioned question and show that no universal upper bound exists for the simulation costs of unsteerable entangled states by examining the lower bound on the simulation cost that has not been previously discussed. Specifically, we prove that  $\gamma(\rho_{AB})$  can be unbounded by showing that its lower bound diverges to infinity, even for two-qubit states.

## 3 Simulation Cost of Werner State and Noisy Spin Measurements

The bulk of our analysis focuses on the two-qubit family of Werner states.

$$\omega_r = r|\Psi^-\rangle\langle\Psi^-| + (1-r)\frac{\mathbb{I} \otimes \mathbb{I}}{4}, \quad (3)$$

where  $|\Psi^-\rangle = \sqrt{1/2}(|01\rangle - |10\rangle)$  is the singlet state. Our restriction to this simple family of states may seem like a limitation. However, on the contrary, we show that many interesting features of simulation cost can already be demonstrated using these states, and they are summarized in Table 1. Furthermore, as we explain in this paper, the lower bounds we prove on  $\gamma(\omega_r)$  translate into lower bounds on  $\gamma(\rho_{AB})$  for any unsteerable state  $\rho_{AB}$ . Finally, the elegant mathematical structure of Werner states allows us to equivalently restate the problem of simulating unsteerable Werner states into the problem of simulating noisy spin measurements; this opens a pathway for using

tools in Banach space theory to tackle both problems simultaneously. We proceed now by exploring this equivalence in more detail.

The task of quantum steering is fundamentally related to another quantum phenomenon known as measurement incompatibility [17, 18, 19]. A family of measurements  $\{M_{a|x}\}_{a,x}$  is called compatible or jointly measurable if each measurement in the family can be simulated by a single ‘parent’ POVM  $\{\Pi_\lambda\}_{\lambda \in \Lambda}$  with index set  $\Lambda$  as:

$$M_{a|x} = \sum_{\lambda \in \Lambda} p(a|x, \lambda) \Pi_\lambda \quad \forall a, x \quad (4)$$

for some channel  $p(a|x, \lambda)$  [20, 21]. In the simple case of quantum observables, compatibility amounts to pairwise commutativity, but the latter is not necessary for general POVMs.

Similar to the simulation cost of steering assemblages and bipartite quantum states, Skrzypczyk *et al.* introduced the notion of *compatibility complexity*, which, for a family of compatible measurements, is the smallest number of outcomes  $|\Lambda|$  such that Eq. (4) holds [22]. The notion of compatibility complexity can be understood as the simulation cost of a set of compatible measurements. In the following sections, we will use ‘compatibility complexity’ and ‘simulation cost’ of compatible measurements interchangeably.

The set of noisy spin measurements on a qubit system offers a paradigmatic case study for measurement incompatibility [13, 23]. Let  $\mathcal{P}_r$  denote a family of noisy spin measurements, such that each measurement in  $\mathcal{P}_r$  is a two-outcome POVM  $\{M_{+|r\hat{n}}, M_{-|r\hat{n}}\}$  with  $M_{\pm|r\hat{n}} = \frac{1}{2}(\mathbb{I} \pm r\hat{n} \cdot \vec{\sigma})$ , with  $\hat{n}$  being a normalized Bloch vector and  $r \in [0, 1]$  the noise parameter that effectively shrinks the Bloch sphere down to radius  $r$ . We similarly let  $\mathcal{P}_r^p$  denote the subset of all noisy spin measurements with  $\hat{n}$  confined to the  $x$ - $z$  plane. It has been previously shown that  $\mathcal{P}_r$  is a compatible family iff  $r \in [0, \frac{1}{2}]$  [8, 24], whereas the compatibility range for  $\mathcal{P}_r^p$  is  $r \in [0, \frac{2}{\pi}]$  [23]. We let  $N(r)$  and  $N^p(r)$  denote the simulation costs (i.e. compatibility complexities) for the measurement families  $\mathcal{P}_r$  and  $\mathcal{P}_r^p$  in their respective compatibility regions.

Using the connection between the local hidden state (LHS) model of Werner states and the compatible model of noisy spin measurements [18, 17], one can relate the simulation cost of Werner states to the simulation cost (compatibility complexity) of noisy spin measurements through the following lemma and proposition.

**Lemma 1.**  $\mathcal{P}_r$  can be simulated with an  $n$ -element POVM if and only if the simulation cost of Werner state  $\omega_r$  under *projective measurements* equals  $n$ .

**Proposition 1.**  $\gamma(\omega_r) \geq N(r)$ .

The inequality  $\gamma(\omega_r) \geq N(r)$  follows by their definitions since  $\gamma(\omega_r)$  is the simulation cost of Werner

state under arbitrary POVMs on Alice’s side, which includes projective measurements as a special subfamily. However, strong numerical evidence indicates that simulating all noisy POVMs will be more costly than simulating noisy spin measurement, as we discuss in the appendix G and summarize in the following conjecture.

**Conjecture 1.** The set of noisy qubit POVMs and noisy qubit PVMs (spin measurements) have different simulation costs.

Thus, it appears the above inequality is not tight in general.

Nevertheless, in special case, we further show in the appendix G that this inequality can be saturated for planar measurements.

**Proposition 2.**  $\gamma^p(\omega_r) = N^p(r)$  for  $r \in [0, \frac{2}{\pi}]$ .

In the following sections, we will start by studying the simulation cost of noisy spin measurements. The connections made in Proposition 1 and Proposition 2 will then help us establish results for the simulation cost of two-qubit Werner states. More general results on the simulation cost of arbitrary bipartite states will be discussed in the last part of the paper.

## 4 Compatibility Radius and Its Geometric Characterization

Propositions 1 and 2 directly translate the problem of simulating  $\omega_r$  into the problem of simulating noisy spin measurements  $\mathcal{P}_r$ , denoted as  $N(r)$  as in Eq. (4). In this section, we will turn the quantities around and identify  $R(n)$  as the largest  $r$  such that an  $n$ -outcome POVM can simulate  $\mathcal{P}_r$ . We will refer to  $R(n)$  as the  $n$ -outcome *compatibility radius*. For any  $r, r' \in [0, \frac{1}{2}]$  and integer  $n$ , the definitions of  $R(n)$  and  $N(r)$  imply the relationship

$$r \leq R(n) < r' \Leftrightarrow N(r) \leq n < N(r'). \quad (5)$$

Similarly, we define  $N^p(r)$  for the plane-restricted case, and so  $r \leq R^p(n) < r' \Leftrightarrow N^p(r) \leq n < N^p(r')$ . From Propositions 1 and 2, we can thus attain bounds for  $\gamma(\omega_r)$  and  $\gamma^p(\omega_r)$  through the study of  $R(n)$  and  $R^p(n)$ , and a detailed relation among all these parameters are summarized in Fig. 2 below.

$R(n)$  and  $R^p(n)$  are also of great interest on their own. Previously, studies on  $R(n)$  and  $R^p(n)$  have only been implicitly made in [15, 25, 26], where the LHS models constructed for Werner states and thus compatible models for simulating noisy spin measurements  $\mathcal{P}(r)$  using some specific  $n$ -outcome POVM  $\{\Pi_\lambda\}$  was studied. One could denote  $R(\{\Pi_\lambda\})$  as the largest  $r$  such that  $\{\Pi_\lambda\}$  can simulate  $\mathcal{P}_r$ . However, to obtain  $R(n)$ , one has to maximize over all  $n$ -outcome POVMs,

$$R(n) = \max_{\{\Pi_\lambda\}} R(\{\Pi_\lambda\}). \quad (6)$$

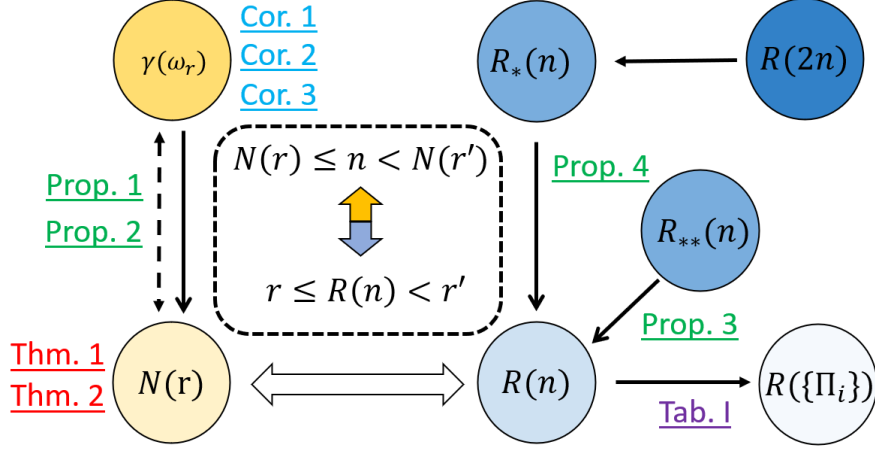


Figure 2: Schematics showing the connections between different quantities in this paper: (a) Left: the relation between simulation cost of Werner states  $\gamma(\omega_r)$  and compatible complexity  $N(r)$  for the set of all noisy spin measurements  $\mathcal{P}_r$ ; (b) Right: the compatible radius for measurements  $R(n)$  and its derivatives, i.e., various lower and upper bounds; (c) The left and right parts are connected by the relation in the middle box; (d)  $\rightarrow$ (dashed): Upper bound from left to right (in special cases).

symbol	Explanation
$\{\Pi_\lambda\}_{\lambda \in \Lambda}$	POVM with effects $\Pi_\lambda$
$\text{sym}\{\Pi_\lambda\}_{\lambda \in \Lambda}$	Symmetric extended POVM
$\Lambda$	Index set of outcome
$\{M_{a x}\}_{a,x}$	Set of Children POVMs
$\gamma(\omega_r)$	Simulation cost of Werner state
$N(r)$	Compatible complexity for noisy spin measurements
$\mathfrak{m}_{\{\Pi_\lambda\}}$	Compatible region of $\{\Pi_\lambda\}$
$\mathfrak{m}_{\{\Pi_\lambda\}}^*$	Compatible region of $\text{sym}\{\Pi_\lambda\}$
$R(\{\Pi_\lambda\})$	Compatible radius for $\{\Pi_\lambda\}$
$R(n)$	$R(\{\Pi_\lambda\})$ for all $n$ -outcome POVM
$R_*(n)$	Symmetric Upper bound of $R(n)$
$R_{**}(n)$	Simplex Upper bound of $R(n)$
$X^p$	Quantity for the planar case

Table 2: Notation used throughout the paper

Furthermore, previous methods for establishing lower bounds on  $R(n)$  have only been computed for small (finite)  $n$  and cannot be generalized to arbitrary  $n$ —let alone provide a non-trivial upper bound. In this work, we offer a comprehensive study of  $R(n)$  by deriving both upper and lower bounds in finite and asymptotic regimes, leveraging various geometric characterizations and inequalities.

Focusing on qubit cases, to compute  $R(\{\Pi_\lambda\})$  for an arbitrary qubit POVM  $\{\Pi_\lambda\}_\lambda$  (and likewise for  $R^p(\{\Pi_\lambda\})$ ) we can express each effect  $\Pi_\lambda$  in the Pauli basis as:

$$\Pi_\lambda = \alpha_\lambda(\mathbb{I} + \eta_\lambda \hat{n}_\lambda \cdot \vec{\sigma}), \quad (7)$$

with  $0 \leq \eta_\lambda, \alpha_\lambda \leq 1$ , and normalization constraints

$$\sum_\lambda \alpha_\lambda = 1 \text{ and } \sum_\lambda \alpha_\lambda \eta_\lambda \hat{n}_\lambda = \vec{0}^T.$$

From a geometric perspective,  $R(\{\Pi_\lambda\})$  can be determined by

$$R(\{\Pi_\lambda\}) := \sup\{r \geq 0 : B(0, r) \subseteq \mathfrak{m}_{\{\Pi_\lambda\}}\},$$

where  $B(0, r) = \{x : \|x\| \leq r\}$ , that is, the largest  $r$  such that the shrunken Bloch sphere of radius  $r$  belongs to the set

$$\mathfrak{m}_{\{\Pi_\lambda\}} = \left\{ 2 \sum_\lambda q_\lambda \alpha_\lambda \hat{n}_\lambda \mid 0 \leq q_\lambda \leq 1, \sum_\lambda q_\lambda \alpha_\lambda = \frac{1}{2} \right\}.$$

The set  $\mathfrak{m}_{\{\Pi_\lambda\}}$  represents the compatible region consisting of all unbiased measurements that can be simulated by  $\{\Pi_\lambda\}$ . By dropping the constraint  $\sum_\lambda q_\lambda \alpha_\lambda = \frac{1}{2}$ , we have an outer approximation set given by

$$\mathfrak{m}_{\{\Pi_\lambda\}}^* = \left\{ 2 \sum_\lambda q_\lambda \alpha_\lambda \hat{n}_\lambda \mid 0 \leq q_\lambda \leq 1 \right\},$$

which, as we discuss in the Appendix A, can also be interpreted as the compatible region of the  $2n$ -outcome POVM  $\text{sym}\{\Pi_\lambda\}_\lambda$  symmetrized form of  $\{\Pi_\lambda\}$ ,

$$\text{sym}\{\Pi_\lambda\}_\lambda := \left\{ \frac{\alpha_\lambda}{2}(\mathbb{I} + \hat{n}_\lambda \cdot \vec{\sigma}), \frac{\alpha_\lambda}{2}(\mathbb{I} - \hat{n}_\lambda \cdot \vec{\sigma}) \right\}_\lambda.$$

The set  $\mathfrak{m}_{\{\Pi_\lambda\}}^*$  is a special convex polytope called a zonotope generated by vectors  $\{2\alpha_\lambda \hat{n}_\lambda\}$  [27, 28], denote  $\text{inr}(S)$  as the inradius of a general convex set. We can thus obtain a very useful geometric characterization on the quantity  $R(n)$  as:

$$R(n) \leq \max_{\{\Pi_\lambda\}_{i=1}^n} \text{inr}(\mathfrak{m}_{\{\Pi_\lambda\}}^*) =: R_*(n) \leq R(2n), \quad (8)$$

which can be used to determine both the lower and upper bounds of  $R(n)$ .

<sup>1</sup>In the appendix D, we further show that it is sufficient to consider  $\eta_\lambda = 1$  when optimizing over all  $R(\{\Pi_\lambda\})$

## 5 Lower Bound on Simulation Cost

From Eq. (5), we obtain lower bounds on  $N(r)$  through upper bounds on  $R(n)$  (thus also on  $\gamma(\omega_r)$  from Proposition 1). In the following, we will provide different lower bounds results on  $R(n)$ , which all rely on various different geometric characterizations of  $R(\{\Pi_\lambda\})$  and  $\mathbf{m}_{\{\Pi_\lambda\}}$ .

We first focus on the case of  $n = 3$ , where a tight upper bound can be determined using a simple geometrical argument.

**Proposition 3.**  $R^p(3) = \frac{1}{2}$  and  $R(4) = \frac{1}{3}$ .

*Proof.* The well-known circumradius-inradius inequality states that the inradius of an  $n$ -simplex is at least  $n$  times smaller than its circumradius [29]. To apply this, consider any three-outcome POVM  $\{\Pi_\lambda\}_{\lambda=1}^3$ . Observe that the set  $\mathbf{m}_{\{\Pi_\lambda\}}$  is contained within the 2-simplex, i.e.,

$$\mathbf{m}_{\{\Pi_\lambda\}} \subseteq \mathbf{m}_{\{\Pi_\lambda\}}^{**} = \left\{ \sum_{\lambda=1}^3 p_\lambda \hat{n}_\lambda \mid \sum_{\lambda=1}^3 p_\lambda = 1 \right\},$$

which has a circumradius equal to one, as the  $\hat{n}_\lambda$  are unit vectors. Therefore, the circumradius-inradius inequality we prove in the Appendix D implies that:

$$R^p(3) \leq \max_{\{\Pi_\lambda\}_{\lambda=1}^3} \text{inr}(\mathbf{m}_{\{\Pi_\lambda\}}^{**}) =: R_{**}(3) \leq \frac{1}{2}.$$

A similar argument for four-outcome POVMs on the full Bloch sphere shows that  $R(4) \leq \frac{1}{3}$ . Combined with the lower bounds of  $R(n)$  in the next section (see Table 3), we have the proposition established.  $\square$

**Corollary 1.** For any  $r > \frac{1}{3}$ , we have  $\gamma(\omega_r) > 4$ . The simulation cost of any entangled Werner state is strictly greater than that of a separable Werner state.

Unfortunately, the outer approximation  $R_{**}(n)$  is too loose for arbitrary  $n$ . To handle the case of  $n > 4$  for planar measurements, we can apply the isoperimetric inequality of polygons to obtain the following.

**Proposition 4.** For  $n$ -outcome planar measurement  $R^p(n) \leq R_*^p(n) = \frac{1}{n} \cot(\frac{\pi}{2n})$ .

*Proof.* Let  $\{\Pi_\lambda\}_{\lambda=1}^n$  be an arbitrary  $n$ -outcome planar POVM. According to Eq. (8), its compatible radius will be upper bounded by the inscribed radius  $\mathbf{m}_{\{\Pi_\lambda\}}^*$ , i.e.,

$$R^p(n) \leq R_*^p(n) = \sup_{\{\Pi_\lambda\}} \text{inr}(\mathbf{m}_{\{\Pi_\lambda\}}^*) \leq \max_{\{\alpha_\lambda \hat{n}_\lambda\}} \frac{2A}{L}, \quad (9)$$

where  $A$  is the area of a  $2n$ -sided zonogon with generators  $\{2\alpha_\lambda \hat{n}_\lambda\}$  and perimeter  $L = 4 \sum_\lambda \alpha_\lambda = 4$  (This perimeter always holds, since the polygon consists of  $n$

pairs of sides parallel to its generators). The isoperimetric inequality of a such a  $2n$ -sided polygon [30] stipulates that

$$A \leq \frac{L^2}{8n \tan(\frac{\pi}{2n})}. \quad (10)$$

Therefore, we have the upper bound

$$R^p(n) \leq \frac{1}{n} \cot(\frac{\pi}{2n}) < \frac{2}{\pi} \quad (11)$$

$\square$

By considering a Taylor expansion of  $x \cot x$  about  $x = 0$ , we observe the inequality  $\frac{1}{n} \cot(\frac{\pi}{2n}) \leq \frac{2}{\pi} (1 - \frac{1}{3} (\frac{\pi}{2n})^2)$ . Setting  $r' = \frac{2}{\pi} (1 - \frac{1}{3} (\frac{\pi}{2n})^2)$ , we apply Eq. (5) and Proposition 2 to reach Corollary 2.

**Corollary 2.** For any  $r \in [0, \frac{2}{\pi}]$ ,

$$\gamma^p(\omega_r) = N^p(r) \geq \sqrt{\frac{\pi}{6}} \left( \frac{2}{\pi} - r \right)^{-\frac{1}{2}}. \quad (12)$$

For noisy spin measurements on the full Bloch sphere  $\mathcal{P}_r$ , we rely on more sophisticated isoperimetric inequalities of zonotopes [31, 32]. The culminating result is stated in the following theorem and discussed in detail in the appendix C.

**Theorem 1.** For any  $r \in [0, \frac{1}{2}]$ ,

$$\gamma(\omega_r) \geq N(r) > c \left( \frac{1}{2} - r \right)^{-\frac{2}{5}} \quad (13)$$

for some positive constant  $c$ .

Both Corollary 2 and Theorem 1 establish our primary claim that the simulation cost of an unsteerable entangled state diverges at  $r = \frac{1}{2}$  (resp.  $\frac{2}{\pi}$ ) when considering general measurements (resp. planar measurements).

## 6 Upper bound on the simulation cost

We now turn to the problem of upper bounding the simulation cost of unsteerable Werner state  $\omega_r$ . Propositions 1 and 2 can again be used to partially solve this problem. Namely, whenever Alice performs projective measurements or planar POVMs we have that the result assemblage  $\mathcal{A}$  can be simulated by shared randomness of size  $N(r)$  and  $N^p(r)$  respectively. What about the most general setting of arbitrary POVMs on Alice's side? Unfortunately, our developed methods appear insufficient to tackle this case, and we leave the full upper bounding as an open problem. However, we note that even if simulating general POVMs requires more shared randomness than simulating just projective measurements, the unsteerability range is the same. That is, as we

have shown in a recent paper,  $\omega_r$  is unsteerable under arbitrary POVMs  $r \in [0, \frac{1}{2}]$  [33].

Like before, we use Eq. (5) and turn the problem of upper bounding  $N(r)$  into lower bounding  $R(n)$ . The latter is further lower bounded by  $R(\{\Pi_\lambda\})$  for any specific parent POVM  $\{\Pi_\lambda\}$ . The same reasoning holds for the planar case.

As discussed and detailed in the appendix D, the compatible radius  $R(\{\Pi_\lambda\})$  of any given qubit measurement  $\Pi_\lambda$ , written in the form of Eq. 7, can be efficiently computed using the following optimization-based criterion:

**Proposition 5.** For a given POVM  $\Pi_\lambda$ , the compatible radius  $R(\{\Pi_\lambda\})$  is given by:

$$R(\{\Pi_\lambda\}) = \inf_{\substack{|\vec{c}|=1 \\ -1 \leq c_0 \leq 1}} \sum_\lambda |\alpha_\lambda(c_0 + \eta_\lambda \vec{c} \cdot \hat{n}_\lambda)|. \quad (14)$$

Thus, when taking the supremum over all  $n$ -outcome POVMs  $\Pi_\lambda$ , the compatibility radius  $R(n)$  can be expressed as:

$$R(n) = \sup_{\Pi_\lambda} \inf_{\substack{|\vec{c}|=1 \\ -1 \leq c_0 \leq 1}} \sum_\lambda |\alpha_\lambda(c_0 + \eta_\lambda \vec{c} \cdot \hat{n}_\lambda)|, \quad (15)$$

and an inconclusive optimization provides a lower bound on  $R(n)$ .

## 6.1 Qubit planar measurements

In general, to obtain the exact value of  $R(n)$  (which can then be translated into an upper bound on  $N(r)$ ), one must optimize over all  $n$ -outcome measurements  $\{\Pi_\lambda\}_{\lambda=1}^n$ . However, a well-chosen  $n$ -outcome measurement  $\{\Pi_\lambda\}_{\lambda=1}^n$  can already provide a relatively tight lower bound on  $R(n)$ .

Intuitively, POVMs  $\{\Pi_\lambda\}_{\lambda=1}^n$  with a large compatible radius are those that are "symmetric." For example, consider qubit planar measurements. We first examine the rotationally symmetric planar POVM  $\{\Pi_\lambda^{\text{rot}} = \frac{1}{n}(\mathbb{I} + \hat{n}_\lambda \cdot \vec{\sigma})\}_{\lambda=1}^n$ , where  $\hat{n}_\lambda = (\cos(\frac{2\pi\lambda}{n}), 0, \sin(\frac{2\pi\lambda}{n}))^T$  [13]. In the appendix, we analytically determine the compatibility radius to be

$$R^p(\{\Pi_\lambda^{\text{rot}}\}) = \begin{cases} \frac{1}{n} \cot(\frac{\pi}{2n}) \cos(\frac{\pi}{2n}) & \text{if } n \text{ is odd} \\ \frac{2}{n} \cot(\frac{\pi}{n}) & \text{if } n \text{ is even} \end{cases}, \quad (16)$$

and simulation models with these parent POVMs are explicitly constructed in the appendix. Similar to the proof of Corollary 2, a Taylor expansion on  $\frac{1}{n} \cot(\frac{\pi}{2n}) \cos(\frac{\pi}{2n})$  allows us to lower bound  $R^p(\{\Pi_\lambda^{\text{rot}}\}) \leq R^p(n)$ , from which Eq. (5) and Proposition 2 can be applied to obtain the following upper bound of  $N^p(r)$  and  $\gamma^p(\omega_r)$ :

**Corollary 3.** For any  $r \in [0, \frac{2}{\pi}]$ ,

$$\gamma^p(\omega_r) = N^p(r) \leq \sqrt{\frac{5\pi}{12}} \left( \frac{2}{\pi} - r \right)^{-\frac{1}{2}} + 1, \quad (17)$$

n	Planar $R^p(n)$		General $R(n)$	
	Symmetric	Numerics	Thomson	Numerics
3	0.5	0.5	0	0
4	0.5	0.5274	0.3333	0.3333
5	0.5854	0.5854	0.3464	0.3718
6	0.5774	0.5927	0.3333	0.4004
7	0.6102	0.6102	0.2857	0.4060
8	0.6035	0.6111	0.4392	
9	0.6206	0.6206	0.4446	
10	0.6155	0.6213	0.4376	
11	0.6259	0.6259	—	
12	0.6220	0.6265	0.4588	

Table 3: Lower bounds on the compatible radii  $R^p(n)$  and  $R(n)$ . For the planar case, the first column describes the largest radius achievable by symmetric POVMs, as given by Eq. (16). For the general case, the third column provides a lower bound on  $R(n)$  using solutions to the Thompson problem, while tighter numerical bounds are obtained by random sampling the parent POVM  $\{\Pi_\lambda\}$  [35].

where the  $+1$  term is needed since  $R^p(\{\Pi_\lambda^{\text{rot}}\})$  does not monotonically increase with  $n$ .

This surprisingly non-monotonic feature implies that symmetric POVMs do not always have the largest compatibility radius, disproving a common suggestion in the literature [16, 34], where symmetric parent POVMs were typically used to construct compatible models (or, similarly, symmetric state ensembles were used when constructing local hidden state models). We have further confirmed this numerically by searching over arbitrary parent POVMs.

As shown in Table 3, for even  $n$ , a non-symmetric POVM can outperform the rotationally symmetric one. Nevertheless, a comparison of Corollaries 2 and 3 demonstrates that  $\{\Pi_\lambda^{\text{rot}}\}_{\lambda=1}^n$  is nearly optimal for simulating noisy spin measurements in the  $x$ - $z$  plane.

## 6.2 General qubit measurements

Next, we turn to simulating all noisy spin measurements. In this general scenario, the rotationally symmetric planar POVM  $\{\Pi_\lambda^{\text{rot}}\}$  cannot be directly generalized, as noisy spin measurements are no longer represented by a shrunken 2D disk but rather a 3D shrunken ball in the Bloch sphere representation. To address this, we consider alternative symmetric constructions for general qubit measurements, based on the idea of "evenly distributing" points on a sphere.

First, we utilize the equally-spaced points obtained from the Thompson problem [36]. The numerical results for  $n \in \{4, \dots, 12\}$  are shown in Table 3. Second, we construct a parent POVM by leveraging the

symmetries of Platonic solids. A detailed analysis of this approach is provided in the appendix E, with results summarized in Table 4.

$n$	POVM $\{\Pi_\lambda\}$	$\mathcal{R}(\{\Pi_\lambda\})$
4	tetrahedron	$\frac{1}{3}$
6	Octahedron	$\frac{1}{3}$
8	Cube	$\frac{\sqrt{6}}{6}$
12	Icosahedron	$\frac{\phi^3 \sqrt{1+(1-\phi)^2}}{3(1+\phi^2)}$
20	Dodecahedron	$\sqrt{\frac{5}{6}} \frac{\phi^2}{5}$

Table 4: Parent POVM with platonic configuration and their associated unbiased compatible region  $\mathbf{m}_{\{\Pi_\lambda\}}$ , where  $\phi = \frac{1+\sqrt{5}}{2}$  is the golden ratio.

The final and most powerful construction leverages results from Refs. [31, 37] on zonotope approximations. These works discuss how to achieve the best approximation of a unit ball using a zonotope generated by a finite number of generators. This is particularly relevant because the compatible region  $\mathbf{m}_{\{\Pi_\lambda\}}^*$  mentioned earlier in the preliminaries is, in fact, a zonotope.

A detailed discussion on zonotopes is provided in the appendix, and the key result is summarized in the following.

**Theorem 2.** For any  $r \in [0, \frac{1}{2}]$ ,

$$N(r) \leq C \left( \frac{1}{2} - r \right)^{-\frac{4}{5}} \quad (18)$$

for some positive constants  $C$ . However, this does not directly provide an upper bound for the simulation cost of  $\gamma(\omega_r)$ , as Proposition 1 is not an equality.

## 7 Simulating Cost of General Unsteerable States

Corollary 1 shows that the separability threshold for two-qubit Werner states coincides with a jump in shared randomness cost from 2 to  $\log_2 5$  bits. In fact, this connection between separability and simulation cost holds for all two-qubit states  $\rho_{AB}$ . That is,  $\gamma(\rho_{AB}) > 4$  if and only if  $\rho_{AB}$  is entangled. As explained in the appendix, this previously unrecognized result actually follows directly from two different results in quantum information theory. First, it happens that for two-qubit separable states, the number of product states needed in a separable decomposition is always at most 4 [38, 39]. Second, Jevtic *et al.* have provided a ‘nested tetrahedron’ condition [40], which, when combined with the ‘four-packable’ condition by Nguyen and Vu [41], says the following.

**Lemma 2** ([40]). A two-qubit state  $\rho_{AB}$  is separable if and only if its steering ellipsoid  $\mathcal{E}_A$  fits inside a tetrahedron that fits inside the Bloch sphere

To be more precise, the steering ellipsoid  $\mathcal{E}_A$  for a bipartite state  $\rho_{AB}$  is defined by first transforming  $\rho_{AB}$  to  $\tilde{\rho}_{AB} \propto (\frac{1}{2} \otimes (\rho_B)^{-1/2}) \rho_{AB} (\frac{1}{2} \otimes (\rho_B)^{-1/2})$  with  $\rho_B = \text{Tr}_A[\rho_{AB}]$ . The possible states that it can be steered to, using the measurement effects  $M_{\pm|\hat{n}} = \frac{1}{2}(\mathbb{I} \pm \mathbf{n} \cdot \boldsymbol{\sigma})$  are given as

$$\tilde{\rho}_{AB} = \begin{pmatrix} 1 & \mathbf{0} \\ \tilde{\mathbf{a}} & \tilde{T} \end{pmatrix} \xrightarrow{M_{\pm|\mathbf{n}}} \sigma_{\pm|\mathbf{n}x} = \frac{1}{2} \begin{pmatrix} 1 & \\ \tilde{\mathbf{a}} \pm \tilde{T}\mathbf{n} & \end{pmatrix} \quad (19)$$

The steering ellipsoid is then defined as the set

$$\mathcal{E}_A = \{\tilde{\mathbf{a}} + \tilde{T}\mathbf{n}\}_{\mathbf{n}} \quad (20)$$

**Proposition 6.**  $\rho_{AB}$  is entangled if and only if  $\gamma(\rho_{AB}) > 4$ .

*Proof.* The ‘only if’ part follows from directly from the existence of minimal separable decompositions for two-qubit state [38, 39], which is always less than 4.

The ‘if’ part can also be simply proved by contradiction. Since  $\rho_{AB}$  is entangled but has a simulation cost less of equal to 4. Then there exists a set of local hidden states  $\{\rho_\lambda = \frac{1}{2}(\mathbb{I} + \mathbf{n}_\lambda \cdot \boldsymbol{\sigma})\}_{\lambda=1}^4$  such that:

$$\begin{aligned} \sigma_{\pm|\mathbf{n}} &= \sum_{i=1}^4 p(\pm|\mathbf{n}, \lambda) p(\lambda) \rho_i \\ \Rightarrow \mathcal{E}_A &= \{\tilde{\mathbf{a}} + \tilde{T}\mathbf{n}\}_{\mathbf{n}} \subseteq \text{Conv}[\mathbf{n}_\lambda]_{\lambda=1}^4. \end{aligned} \quad (21)$$

This essentially shows that there exists a tetrahedron defined by the Bloch vectors  $\{\mathbf{n}_\lambda\}_{\lambda=1}^4$  of  $\{\rho_\lambda\}_{\lambda=1}^4$  that contain the ellipsoid  $\mathcal{E}_A$ . Thus,  $\tilde{\rho}_{AB}$  is entangled from Lemma 2, and there is a contradiction.

Thus, we conclude that  $\rho_{AB}$  is entangled if and only if  $\gamma(\rho_{AB}) > 4$ .  $\square$

We now discuss ways in which our results can be applied to unsteerable states beyond the two-qubit Werner family. Observe that any unsteerable state  $\rho_{AB}$  will satisfy  $\gamma(\rho) \geq \gamma(\mathcal{L}(\rho)) - m$  under any map of the form  $\mathcal{L} = \sum_{i=1}^m \mathcal{N}_i \otimes \mathcal{E}_i$ , where the  $\mathcal{N}_i$  are completely positive and trace-preserving (CPTP) map while the  $\mathcal{E}_i$  are just CP [42]. Hence, we can lower bound the simulation cost of  $\rho_{AB}$  by first transforming it to a two-qubit state using the map above. Secondly, it is well-known that every two-qubit state can be converted into a Werner state when Alice and Bob simultaneously apply one of twelve random Clifford gates to their system (a so-called ‘twirling map’) [43]. Moreover, the noise parameter  $r$  in the resulting state is given by the singlet fraction, i.e.  $\rho \mapsto \rho_W(r)$  with  $r = \langle \Phi^- | \rho | \Phi^- \rangle - \frac{1}{4}$ . Since the twirling map will increase the shared randomness in a LHS model by a

factor of twelve, we conclude that any unsteerable state  $\rho_{AB}$  with  $\langle \Phi^- | \mathcal{L}(\rho) | \Phi^- \rangle > R(n)$  will require a LHS model with at least  $\log_2 n - \log_2(12m)$  bits of shared randomness. From Theorem 1, this amount grows unbounded as  $\langle \Phi^- | \mathcal{L}(\rho) | \Phi^- \rangle \rightarrow 3/4$ , which corresponds to the threshold  $r = \frac{1}{2}$  for Werner states.

*Conclusions* – In this work we studied the shared randomness cost  $\gamma(\rho_{AB})$  for simulating c-to-cq channels built using  $\rho_{AB}$ . We characterized the simulation cost and showed that it can be unbounded. The mathematical methods we developed to study this problem used the correspondence between steerability and measurement incompatibility and their similar geometric picture. Analogous to any other type of channel simulation cost, the quantity  $\gamma(\rho_{AB})$  provides one measure of operational resourcefulness for every unsteerable state  $\rho$ . Furthermore, understanding the simulation cost of different assemblages can be used for semi-device-independent entanglement verification [9] when Alice and Bob are known to have a limited amount of shared randomness, even in noisy environments where quantum steering is not possible.

The results presented here pertain to LHS models. As future work, it would be interesting if similar techniques can be applied to bound the shared randomness needed for local hidden variable (LHV) models. Since LHS models are more demanding than LHV models, the upper bounds presented in this work will still apply.

Finally, we close by conjecturing a more fundamental role for the simulation cost  $\gamma(\rho_{AB})$  in the study of nonlocality and entanglement. The notion of steerability provides a clean partitioning in the set of bipartite quantum states between those that are steerable versus those that are not. However, this partition does not coincide with the separation between entangled and separable states [44, 8]. In contrast, we have found here that the for two-qubit states the jump from separable to entangled-unsteerable coincides with a jump in the simulation cost. Hence, by moving beyond steering and focusing on simulation cost, we recover the separable/entangled boundary. Perhaps such a relationship holds for higher-dimensional bipartite states as well.

*Acknowledgements* – This work was supported by NSF Award 1839177. The authors thank Virginia Lorenz and Marius Junge for helpful discussions during the preparation of this manuscript.

## References

[1] Toby S. Cubitt, Debbie Leung, William Matthews, and Andreas Winter. Improving zero-error classical communication with entanglement. *Phys. Rev. Lett.*, 104:230503, Jun 2010.

[2] Debbie Leung, Laura Mancinska, William Matthews, Maris Ozols, and Aidan Roy. Entanglement can increase asymptotic rates of zero-error classical communication over classical channels. *Communications in Mathematical Physics*, 311(1):97–111, March 2012.

[3] Charles H. Bennett, Gilles Brassard, Claude Crépeau, Richard Jozsa, Asher Peres, and William K. Wootters. Teleporting an unknown quantum state via dual classical and einstein-podolsky-rosen channels. *Phys. Rev. Lett.*, 70:1895–1899, Mar 1993.

[4] C.H. Bennett, P.W. Shor, J.A. Smolin, and A.V. Thapliyal. Entanglement-assisted capacity of a quantum channel and the reverse shannon theorem. *IEEE Transactions on Information Theory*, 48(10):2637–2655, October 2002.

[5] Toby S. Cubitt, Debbie Leung, William Matthews, and Andreas Winter. Zero-error channel capacity and simulation assisted by non-local correlations. *IEEE Transactions on Information Theory*, 57(8):5509–5523, August 2011.

[6] David Schmid, Denis Rosset, and Francesco Buscemi. The type-independent resource theory of local operations and shared randomness. *Quantum*, 4:262, April 2020.

[7] Roope Uola, Ana C. S. Costa, H. Chau Nguyen, and Otfried Gühne. Quantum steering. *Rev. Mod. Phys.*, 92:015001, Mar 2020.

[8] H. M. Wiseman, S. J. Jones, and A. C. Doherty. Steering, entanglement, nonlocality, and the einstein-podolsky-rosen paradox. *Phys. Rev. Lett.*, 98:140402, Apr 2007.

[9] D Cavalcanti and P Skrzypczyk. Quantum steering: a review with focus on semidefinite programming. *Reports on Progress in Physics*, 80(2):024001, dec 2016.

[10] Marco Piani and John Watrous. Necessary and sufficient quantum information characterization of einstein-podolsky-rosen steering. *Phys. Rev. Lett.*, 114:060404, Feb 2015.

[11] Joseph Bowles, Tamás Vértesi, Marco Túlio Quintino, and Nicolas Brunner. One-way einstein-podolsky-rosen steering. *Phys. Rev. Lett.*, 112:200402, May 2014.

[12] Joseph Bowles, Flavien Hirsch, Marco Túlio Quintino, and Nicolas Brunner. Sufficient criterion for guaranteeing that a two-qubit state is unsteerable. *Phys. Rev. A*, 93:022121, Feb 2016.

[13] Jessica Bavaresco, Marco Túlio Quintino, Leonardo Guerini, Thiago O. Maciel, Daniel Cavalcanti, and Marcelo Terra Cunha. Most incompatible measurements for robust steering tests. *Phys. Rev. A*, 96:022110, Aug 2017.

[14] Armin Uhlmann. *Open Systems Information Dynamics*, 5(3):209–228, 1998.

[15] Joseph Bowles, Flavien Hirsch, Marco Túlio Quintino, and Nicolas Brunner. Local hidden variable models for entangled quantum states using finite shared randomness. *Phys. Rev. Lett.*, 114:120401, Mar 2015.

[16] H. Chau Nguyen, Huy-Viet Nguyen, and Otfried Gühne. Geometry of einstein-podolsky-rosen correlations. *Phys. Rev. Lett.*, 122:240401, Jun 2019.

[17] Marco Túlio Quintino, Tamás Vértesi, and Nicolas Brunner. Joint measurability, einstein-podolsky-rosen steering, and bell nonlocality. *Phys. Rev. Lett.*, 113:160402, Oct 2014.

[18] Roope Uola, Tobias Moroder, and Otfried Gühne. Joint measurability of generalized measurements implies classicality. *Phys. Rev. Lett.*, 113:160403, Oct 2014.

[19] Nicolas Brunner, Daniel Cavalcanti, Stefano Pironio, Valerio Scarani, and Stephanie Wehner. Bell nonlocality. *Rev. Mod. Phys.*, 86:419–478, Apr 2014.

[20] Teiko Heinosaari, Takayuki Miyadera, and Mário Ziman. An invitation to quantum incompatibility. *Journal of Physics A: Mathematical and Theoretical*, 49(12):123001, February 2016.

[21] Leonardo Guerini, Jessica Bavaresco, Marcelo Terra Cunha, and Antonio Acín. Operational framework for quantum measurement simulability. *Journal of Mathematical Physics*, 58(9):092102, September 2017.

[22] Paul Skrzypczyk, Matty J. Hoban, Ana Belén Sainz, and Noah Linden. Complexity of compatible measurements. *Phys. Rev. Research*, 2:023292, Jun 2020.

[23] Roope Uola, Kimmo Luoma, Tobias Moroder, and Teiko Heinosaari. Adaptive strategy for joint measurements. *Phys. Rev. A*, 94:022109, Aug 2016.

[24] Teiko Heinosaari, Jukka Kiukas, Daniel Reitzner, and Jussi Schultz. Incompatibility breaking quantum channels. *Journal of Physics A: Mathematical and Theoretical*, 48(43):435301, oct 2015.

[25] Flavien Hirsch, Marco Túlio Quintino, Tamás Vértesi, Matthew F. Pusey, and Nicolas Brunner. Algorithmic construction of local hidden variable models for entangled quantum states. *Phys. Rev. Lett.*, 117:190402, Nov 2016.

[26] D Cavalcanti and P Skrzypczyk. Quantum steering: a review with focus on semidefinite programming. *Reports on Progress in Physics*, 80(2):024001, dec 2016.

[27] Peter McMullen. On zonotopes. *Transactions of the American Mathematical Society*, 159:91–109, 1971.

[28] Günter M Ziegler. *Lectures on polytopes*, volume 152. Springer Science & Business Media, 2012.

[29] Murray S. Klamkin and George A. Tsintsifas. The circumradius-inradius inequality for a simplex. *Mathematics Magazine*, 52(1):20–22, 1979.

[30] Viktor Blåsjö. The isoperimetric problem. *The American Mathematical Monthly*, 112(6):526–566, 2005.

[31] J. Bourgain and J. Lindenstrauss. Distribution of points on spheres and approximation by zonotopes. *Israel Journal of Mathematics*, 64(1):25–31, Feb 1988.

[32] Jean Bourgain and Joram Lindenstrauss. Approximating the ball by a minkowski sum of segments with equal length. *Discrete & Computational Geometry*, 9(2):131–144, Feb 1993.

[33] Yujie Zhang and Eric Chitambar. Exact steering bound for two-qubit werner states. *Phys. Rev. Lett.*, 132:250201, Jun 2024.

[34] Reinhard F. Werner. Quantum states with einstein-podolsky-rosen correlations admitting a hidden-variable model. *Phys. Rev. A*, 40:4277–4281, Oct 1989.

[35] Yujie Zhang. Compatible radius calculation. <https://github.com/yujie4phy/Compatible-radius-calculation.git>, 2023.

[36] David J. Wales and Sidika Ulker. Structure and dynamics of spherical crystals characterized for the thomson problem. *Phys. Rev. B*, 74:212101, Dec 2006.

[37] Jonathan W. Siegel. Optimal approximation of zonoids and uniform approximation by shallow neural networks, 2023.

[38] Anna Sanpera, Rolf Tarrach, and Guifré Vidal. Local description of quantum inseparability. *Phys. Rev. A*, 58:826–830, Aug 1998.

[39] William K. Wootters. Entanglement of formation of an arbitrary state of two qubits. *Phys. Rev. Lett.*, 80:2245–2248, Mar 1998.

[40] Sania Jevtic, Matthew Pusey, David Jennings, and Terry Rudolph. Quantum steering ellipsoids. *Phys. Rev. Lett.*, 113:020402, Jul 2014.

[41] H. Chau Nguyen and Thanh Vu. Nonseparability and steerability of two-qubit states from the geometry of steering outcomes. *Phys. Rev. A*, 94:012114, Jul 2016.

[42] Rodrigo Gallego and Leandro Aolita. Resource theory of steering. *Phys. Rev. X*, 5:041008, Oct 2015.

[43] D.P. DiVincenzo, D.W. Leung, and B.M. Terhal. Quantum data hiding. *IEEE Transactions on Information Theory*, 48(3):580–598, March 2002.

- [44] Jonathan Barrett. Nonsequential positive-operator-valued measurements on entangled mixed states do not always violate a bell inequality. *Phys. Rev. A*, 65:042302, Mar 2002.
- [45] Constrained zonotopes: A new tool for set-based estimation and fault detection. *Automat-ica*, 69:126–136, 2016.
- [46] J. Bourgain, J. Lindenstrauss, and V. Milman. Approximation of zonoids by zonotopes. *Acta Mathematica*, 162(none):73 – 141, 1989.

# Appendix

<b>A</b> <b>Geometry of compatible region</b>	<b>11</b>
<b>B</b> <b>Proof of proposition 3, and Corollary 1</b>	<b>12</b>
<b>C</b> <b>Proof of Theorem 1, Theorem 2 and connection to Zonotope approximation</b>	<b>13</b>
<b>D</b> <b>Criterion for compatible radius <math>R(\{\Pi_\lambda\})</math></b>	<b>14</b>
<b>E</b> <b>Example of <math>R(\{\Pi_\lambda\})</math> for symmetric POVMs, and compatible models</b>	<b>16</b>
<b>F</b> <b>Simulation cost of entangled state and compatible measurements</b>	<b>20</b>
<b>G</b> <b>Discussion on prop. 1, prop. 2 and conj. 1</b>	<b>20</b>
1    Inequivalence between simulation cost of PVMs and POVMs . . . . .	20
2    Equivalence between simulation cost of PVMs and POVMs for qubit planar measurements . . . . .	22

Here we provide some technical detail that complements the main manuscript.

In section [A](#) we establish a detailed geometrical connection between our problem and the analysis of zonotopes, a special types of convex polytope.

In section [B](#), we prove prop. [3](#) and cor. [1](#) of the main text related to the first geometric inequality - the circumradius-inradius inequality we use

In section [C](#), we connect our problem to the zonotope approximation problems and thm [1](#) and thm [2](#) are proven.

In section [D](#), we provide an optimization-based criteria. for the computation of compatible radius  $R(\{\Pi_\lambda\})$  for a given  $\{\Pi_\lambda\}$ .

In section [E](#), we give special examples of symmetric POVMs and calculate their compatibility region  $\mathfrak{m}_{\{\Pi_\lambda\}}$  and compatibility radius  $R(\{\Pi_\lambda\})$  explicitly.

In section [F](#), we establish a connection between our problem and the shared randomness cost in quantum steering.

Finally, we give evidence in Section [G](#) and conjecture that the simulation cost of noisy spin measurements (PVMs) might be strictly smaller than the simulation cost of noisy POVMs.

## A Geometry of compatible region

**Definition 1.** A zonotope is a set of points in  $d$ -dimensional space constructed from vectors  $\{\vec{v}_i\}$  by taking the Minkowski sum of line segments:

$$\mathcal{Z} = \left\{ \sum_\lambda x_\lambda \vec{v}_i \mid 0 \leq x_\lambda \leq 1 \right\},$$

where the set of vectors  $\{\vec{v}_i\}$  is defined as the generator of the zonotope.

With the above notation, we introduce the compatible region  $\mathcal{M}_{\{\Pi_\lambda\}} := \left\{ \sum_\lambda p_\lambda \Pi_\lambda \mid 0 \leq p_\lambda \leq 1 \right\}$ , which is the collection of all effects that can be simulated by  $\{\Pi_\lambda\}$  (or in other words, representing all dichotomic measurement that can be simulated by  $\{\Pi_\lambda\}$ ). This region can be viewed as a zonotope in an  $n^2$ -dimensional Hilbert space of bounded operators [27, 28], where  $n$  is the dimension of the Hilbert space on which the measurement effects act.

For qubit measurements, we can simply the problem by parameterizing a quantum measurement  $\{\Pi_\lambda\}$  in the Pauli basis, which provides a natural way to represent each effect  $\Pi_\lambda = \alpha_\lambda (\mathbb{I} + \hat{n}_\lambda \cdot \vec{\sigma})$  as a 4-dimensional vector:

$$\vec{\pi}_\lambda = (\alpha_\lambda, \alpha_\lambda \hat{n}_\lambda)^T = (\alpha_\lambda, \alpha_\lambda \hat{n}_\lambda^x, \alpha_\lambda \hat{n}_\lambda^y, \alpha_\lambda \hat{n}_\lambda^z)^T. \quad (22)$$

The normalization and positivity constraints are expressed as  $\sum_\lambda \vec{\pi}_\lambda = (1, 0, 0, 0)$  and  $\alpha_\lambda \geq 0$ . Thus, we can geometrically visualize the compatible region for any given measurement in a 4-dimensional Euclidean space:

$$\mathfrak{m}_{\{\Pi_\lambda\}} := \left\{ 2 \sum_\lambda p_\lambda \vec{\pi}_\lambda \mid 0 \leq p_\lambda \leq 1 \right\}, \quad (23)$$

where the factor of 2 is introduced for convenience.

Compared to the 4-dimensional compatible region, there are two 3-dimensional subsets of it that play a crucial role in the study of the simulation cost of noisy spin measurements:  $\mathfrak{m}_{\{\Pi_\lambda\}}$  and  $\mathfrak{m}_{\{\Pi_\lambda\}}^*$  defined in the main text. Both subsets can be derived from this 4-dimensional zonotope and are explained as follows:

**Definition 2.** The *constrained zonotope*  $\mathfrak{m}_{\{\Pi_\lambda\}} := \left\{ 2 \sum_\lambda p_\lambda \hat{n}_\lambda \mid 0 \leq p_\lambda \leq 1, \sum_\lambda p_\lambda \alpha_\lambda = \frac{1}{2} \right\}$  is the three-dimensional cross-section of  $\mathfrak{M}_{\{\Pi_\lambda\}}$  on the plane defined by  $\sum_\lambda p_\lambda \alpha_\lambda = \frac{1}{2}$ . However, this set is not generally a zonotope in general[45]. The set  $\mathfrak{m}_{\{\Pi_\lambda\}}$  represents all unbiased dichotomic measurements (with each effect having the same trace) that can be simulated by  $\{\Pi_\lambda\}$ .

**Definition 3.** The *projected zonotope*  $\mathfrak{m}_{\{\Pi_\lambda\}}^* := \left\{ 2 \sum_\lambda p_\lambda \mathbb{P} \vec{\pi}_\lambda \mid 0 \leq p_\lambda \leq 1 \right\} = \left\{ 2 \sum_\lambda p_\lambda \hat{n}_\lambda \mid 0 \leq p_\lambda \leq 1 \right\}$  is a zonotope, where  $\mathbb{P}$  projects vector  $(x, \vec{y})^T \in \mathbb{R}^4$  onto  $(\vec{y})^T \in \mathbb{R}^3$ . By definition,  $\mathfrak{m}_{\{\Pi_\lambda\}} \subseteq \mathfrak{m}_{\{\Pi_\lambda\}}^*$  with equality holding if  $\{\mathbb{P} \vec{\pi}_\lambda\} = \{(\alpha_\lambda \hat{n}_\lambda)^T\}$  is centrally symmetric. Centrally symmetric measurements are the POVMs  $\text{sym}\{\Pi_\lambda\}$  introduced in the main text.

The introduction of a projected zonotope is meaningful both geometrically and analytically.

- Geometrically, giving any arbitrary POVM  $\{\Pi_\lambda\}$ , we can symmetrically extend it to a new POVM  $\text{sym}\{\Pi_\lambda\} = \{\frac{\Pi_\lambda}{2}, \text{Tri}\Pi_\lambda(\mathbb{I} - \frac{\Pi_\lambda}{2})\}$ . The projected zonotope for the original POVM is actually the constrained zonotope of the new symmetric-extended POVM  $\text{sym}\{\Pi_\lambda\}$ .
- Analytically, when computing the compatibility radius  $R(\{\Pi_\lambda\}) = \inf_{|\vec{c}|=1, -1 \leq c_0 \leq 1} \sum_\lambda |\alpha_\lambda(c_0 + \vec{c} \cdot \hat{n}_\lambda)|$  for the constrained zonotope (see Section D), an upper bound is given by the compatible radius for the projected zonotope:  $R(\{\Pi_\lambda\}) \leq R_*(\{\Pi_\lambda\}) := \inf_{|\vec{c}|=1} \sum_\lambda |\alpha_\lambda(\vec{c} \cdot \hat{n}_\lambda)|$ , which appears to be much easier to characterize in many cases.

## B Proof of proposition 3, and Corollary 1

**Lemma 3** (The circumradius-inradius inequality). The inradius  $r$  of an arbitrary  $n$ -simplex is at least  $n$  times less than its circumradius  $R$ . The inequality saturates when the  $n$ -simplex is regular.

*Proof.* Let  $A_i$  and  $F_i$  (for  $i = 1, 2, \dots, n+1$ ) denote, respectively, the vertices and its opposite  $(n-1)$ -dimensional faces of an  $n$ -dimensional simplex of volume  $V$ . Also, let  $h_i$  and  $\eta_\lambda$  denote the distances from  $A_i$  and circumcenter  $O$  to the  $F_i$ , respectively.

Then  $R + \eta_\lambda \geq h_i$ . Moreover, the volume of the  $n$ -dimensional simplex is given by  $h_i F_i / n$ , and so by evaluating the volume of the simplex in three different ways, we get:

$$nV = h_i F_i = \sum \eta_\lambda F_i = r \sum F_i.$$

Therefore,

$$\sum (R + \eta_\lambda) F_i = (R + r) \sum F_i \geq \sum h_i F_i = (n+1)r \sum F_i \rightarrow R \geq nr$$

□

**Proposition 3.**  $\mathcal{R}^p(3) = \frac{1}{2}$  and  $\mathcal{R}(4) = \frac{1}{3}$ .

*Proof.* To apply Lemma 3, first consider the planar case. Given any three-outcome POVM  $\{\Pi_\lambda\}_{i=1}^3$ , observe that the set  $\mathfrak{m}_{\{\Pi_\lambda\}}$  is contained in the 2-simplex  $\mathfrak{m}_{\{\Pi_\lambda\}}^{**} = \{\sum_{i=1}^3 p_i \hat{n}_\lambda \mid \sum_{i=1}^3 p_i = 1\}$  in two dimensions, with a circumradius equaling one since the  $\hat{n}_\lambda$  are unit vectors. Therefore, the circumradius-inradius inequality implies that

$$\mathcal{R}^p(3) \leq \max_{\{\Pi_\lambda\}_{i=1}^3} \text{inr}(\mathfrak{m}_{\{\Pi_\lambda\}}^{**}) =: \mathcal{R}_{**}^p(3) \leq \frac{1}{2}.$$

A similar argument for four-outcome POVMs on the full Bloch sphere shows that  $\mathcal{R}(4) \leq \frac{1}{3}$ , where now the compatible region  $\mathfrak{m}_{\{\Pi_\lambda\}}$  and three-simplex  $\mathfrak{m}_{\{\Pi_\lambda\}}^{**}$  are in  $\mathbb{R}^3$ . Combined with the lower bounds from Table I in the main text, we have the stated equalities. □

**Corollary 1.** For any  $r > \frac{1}{3}$ , we have  $\gamma(\omega_r) > 4$ . The simulation cost of any entangled Werner state is strictly greater than that of a separable Werner state.

## C Proof of Theorem 1, Theorem 2 and connection to Zonotope approximation

In this section, we will discuss the technical details of applying the well-studied results in approximating Euclidean Balls with Zonotopes to our specific problem.

**Lemma 4.** [46] For any zonotope generated by  $2n$  line segments  $\{\pm\alpha_\lambda \hat{n}_\lambda\}$  with  $\sum_\lambda \alpha_\lambda = 1$ , There exist a positive constant  $c_d$  depending on dimension  $d$  only such that:

$$\left\| \sum_\lambda \alpha_\lambda |\langle \hat{n}_\lambda, \hat{x} \rangle| - \beta_d \right\|_{L^2(S_{d-1})} \geq c_d n^{-\frac{d+2}{2(d-1)}}, \quad (24)$$

where  $\|X\|_{L^2(S_{d-1})} = \sqrt{\int |x|^2 dS_{d-1}}$  is the  $L^2$  norm on the integral of function  $x$  and  $\beta_3 = \frac{1}{2}$ ,  $\beta_2 = \frac{2}{\pi}$ .

The proof is given in detail in [46] based on the spherical harmonic expansion of these quantities.

**Theorem 1.** For any  $n$ -outcome POVM  $\{\Pi_\lambda\}$ , the compatible radius is upper bounded by

$$\begin{aligned} R(n) &\leq \frac{1}{2} - c_3 n^{-\frac{5}{2}} \iff \gamma(\omega_r) \geq c'_3 \left| \frac{1}{2} - r \right|^{-\frac{2}{5}} \\ R^p(n) &\leq \frac{2}{\pi} - c_2 n^{-4} \iff \gamma^p(\omega_r) \geq c'_2 \left| \frac{2}{\pi} - r \right|^{-\frac{1}{4}} \end{aligned} \quad (25)$$

for some positive constant  $c_d$ .

*Proof.* For any  $n$ -outcome POVM  $\{\Pi_\lambda\}$ , we have a chain of inequality given as:

$$R(n) = \max_{\{\Pi_\lambda\}} R(\{\Pi_\lambda\}) \leq \max_{\{\Pi_\lambda\}} R(\text{sym}\{\Pi_\lambda\}) = 2 \max_{\{\alpha_\lambda \hat{n}_\lambda\}} \text{inr}(\mathbf{m}_{\{\Pi_\lambda\}}^*) = \max_{\{\alpha_\lambda \hat{n}_\lambda\}} \min_{\hat{x}} \sum_\lambda \alpha_\lambda |\langle \hat{n}_\lambda, \hat{x} \rangle| \quad (26)$$

(see Eq. (43) for the last equality). From Lemma 4, we have a lower bound on  $\|\sum_\lambda \alpha_\lambda |\langle \hat{n}_\lambda, \hat{x} \rangle| - \beta_d\|_{L^2(S_{d-1})}$ . Using Holder's inequality,

$$\begin{aligned} \left\| \sum_\lambda \alpha_\lambda |\langle \hat{n}_\lambda, \hat{x} \rangle| - \beta_d \right\|_{L^2(S_{d-1})}^2 &\leq \left\| \sum_\lambda \alpha_\lambda |\langle \hat{n}_\lambda, \hat{x} \rangle| - \beta_d \right\|_{L^1(S_{d-1})} \left\| \sum_\lambda \alpha_\lambda |\langle \hat{n}_\lambda, \hat{x} \rangle| - \beta_d \right\|_{L^\infty(S_{d-1})} \\ &\leq \left\| \sum_\lambda \alpha_\lambda |\langle \hat{n}_\lambda, \hat{x} \rangle| - \beta_d \right\|_{L^1(S_{d-1})} \end{aligned} \quad (27)$$

Where  $L^1$ , and  $L^\infty$  stand for the  $L^1$  and  $L^\infty$  norm of the integral of measurable function. Additionally, since  $\int (\sum_\lambda \alpha_\lambda |\langle \hat{n}_\lambda, \hat{x} \rangle| - \beta_d) dS_{d-1} = 0$  implies that

$$\int_{\sum_\lambda \alpha_\lambda |\langle \hat{n}_\lambda, \hat{x} \rangle| < \beta_d} \left| \sum_\lambda \alpha_\lambda |\langle \hat{n}_\lambda, \hat{x} \rangle| - \beta_d \right| dS_{d-1} = \frac{1}{2} \left\| \sum_\lambda \alpha_\lambda |\langle \hat{n}_\lambda, \hat{x} \rangle| - \beta_d \right\|_{L^1}, \quad (28)$$

we therefore have

$$\max_{\hat{x}} \left( \beta_d - \sum_\lambda \alpha_\lambda |\langle \hat{n}_\lambda, \hat{x} \rangle| \right) \geq \frac{1}{2} \left\| \sum_\lambda \alpha_\lambda |\langle \hat{n}_\lambda, \hat{x} \rangle| - \beta_d \right\|_{L^1} \geq \frac{1}{2} \left\| \sum_\lambda \alpha_\lambda |\langle \hat{n}_\lambda, \hat{x} \rangle| - \beta_d \right\|_{L^2}^2 \geq \frac{1}{2} c_d^2 n^{-\frac{d+2}{d-1}}. \quad (29)$$

In the end we have

$$\max_{\{\alpha_\lambda \hat{n}_\lambda\}} \min_{\hat{x}} \sum_\lambda \alpha_\lambda |\langle \hat{n}_\lambda, \hat{x} \rangle| \leq \beta_d - \frac{1}{2} c_d^2 n^{-\frac{d+2}{d-1}}, \quad (30)$$

from which we conclude:

$$\begin{aligned} R(n) &\leq R_*(2n) \leq \frac{1}{2} - c'_3 n^{-\frac{5}{2}} \iff \gamma(\omega_r) \geq c'_3 \left| \frac{1}{2} - r \right|^{-\frac{2}{5}} \\ R^p(n) &\leq R_*^p(2n) \leq \frac{2}{\pi} - c'_2 n^{-4} \iff \gamma^p(\omega_r) \geq c'_2 \left| \frac{2}{\pi} - r \right|^{-\frac{1}{4}} \end{aligned} \quad (31)$$

for some positive constant  $c'_d$

□

**Remark.** The bound here for planar measurements is less tight than the upper bound we obtained in corollary 3.

**Lemma 5** ([37]). There exists a positive constant  $C_d$  and zonotope in  $\mathbb{R}^d$  with  $2n$  generators  $\{\pm\alpha_\lambda \hat{n}_\lambda\}_{i=1}^n$  such that

$$\left| \sum_{i=1}^n \alpha_\lambda |\hat{n}_\lambda \cdot \hat{c}| - \beta_d \right| < C_d n^{-\frac{1}{2} - \frac{3}{2(d-1)}} \quad \forall \hat{c}, \quad (32)$$

where  $\beta_d = \int_{S_{d-1}} \sum_{i=1}^n \alpha_\lambda |\hat{n}_\lambda \cdot \hat{c}| d\hat{c} / \int_{S_{d-1}} d\hat{c}$ , with  $\beta_2 = \frac{2}{\pi}$  and  $\beta_3 = \frac{1}{2}$ .

From Proposition 5, since  $\min_{\hat{c}} \sum_{i=1}^n \alpha_\lambda |(\hat{c} \cdot \hat{n}_\lambda)| \leq \beta_d$  by definition:

$$R(2n) \geq R(\text{sym}\{\Pi_\lambda\}) = \min_{\hat{c}} \sum_{i=1}^n \alpha_\lambda |(\hat{c} \cdot \hat{n}_\lambda)| > \beta_d - C_d n^{-\frac{1}{2} - \frac{3}{2(d-1)}}. \quad (33)$$

We thus immediately obtain an upper bound on the simulation cost:

**Theorem 2.** For  $r < \frac{1}{2}$  (resp.  $r < \frac{2}{\pi}$ ), the simulation cost is upper bounded by:

$$\gamma^p(\omega_r) \leq C'_2 \left| \frac{1}{2} - r \right|^{-4/5} \quad (34)$$

$$\gamma(\omega_r) \leq C'_3 \left| \frac{2}{\pi} - r \right|^{-1/2} \quad (35)$$

for some positive constants  $C'_d$ .

We note that, for planar measurements, the asymptotic limit can also be obtained by taking  $n \rightarrow \infty$  in Eq. 16, which yields:  $R(n) \geq R^p(\{\Pi_\lambda^{\text{rot}}\}) \approx \frac{2}{\pi} - \frac{\pi}{6n^2}$ . Therefore,  $\gamma^p(\omega_r) = N^p(r) \leq \sqrt{\frac{\pi}{6}} \left| \frac{2}{\pi} - r \right|^{-1/2}$

## D Criterion for compatible radius $R(\{\Pi_\lambda\})$

**Proposition 5.** For a given qubit POVM  $\{\Pi_\lambda = \alpha_\lambda (\mathbb{I} + \eta_\lambda \hat{n}_\lambda \cdot \vec{\sigma})\}$ , the compatible radius  $R(\{\Pi_\lambda\})$  is given by:

$$R(\{\Pi_\lambda\}) = \inf_{\substack{|\vec{c}|=1 \\ -1 \leq c_0 \leq 1}} \sum_\lambda |\alpha_\lambda (c_0 + \eta_\lambda \vec{c} \cdot \hat{n}_\lambda)|. \quad (36)$$

*Proof.* We start by noticing that the set  $\mathcal{M}_{\{\Pi_\lambda\}}$  is convex for any given  $\{\Pi_\lambda\}$ . Therefore, we can always find a set of tight inequalities that bound  $\mathcal{M}_{\{\Pi_\lambda\}}$ . Such an inequality can be represented using an operator  $C = c_0 \mathbb{I} + \vec{c} \cdot \vec{\sigma}$ . Let  $N \in \mathcal{M}_{\{\Pi_\lambda\}}$ , then for any  $C$  we can write the inequality as

$$\langle C, N \rangle \leq \max_{M \in \mathcal{M}_{\{\Pi_\lambda\}}} \langle C, M \rangle \quad (37)$$

where  $\langle X, Y \rangle = \text{Tr}[XY]$ .

Given a child POVM  $N = n_0(\mathbb{I} + \vec{n} \cdot \vec{\sigma})$ , we can proceed to simplify the above inequality:

$$\begin{aligned} n_0(c_0 + \vec{c} \cdot \vec{n}) &\leq \sum_\lambda \max_{0 \leq x_\lambda \leq 1} \alpha_\lambda x_\lambda (c_0 + \eta_\lambda \vec{c} \cdot \hat{n}_\lambda) \\ &= \sum_\lambda \max[\alpha_\lambda (c_0 + \eta_\lambda \vec{c} \cdot \hat{n}_\lambda), 0], \end{aligned} \quad (38)$$

where the equality is always attainable by setting  $x_\lambda = 0$  whenever  $c_0 + \eta_\lambda \vec{c} \cdot \hat{n}_\lambda \leq 0$  and  $x_\lambda = 1$  otherwise. Moreover for any  $N \in \mathcal{M}_{\{\Pi_\lambda\}}$ , we have  $n_0 = \frac{1}{2}$ . Therefore, we can simplify the above inequality as:

$$\begin{aligned} \vec{c} \cdot \vec{n} &\leq 2 \sum_\lambda \max[\alpha_\lambda (c_0 + \eta_\lambda \vec{c} \cdot \hat{n}_\lambda), 0] - c_0 = 2 \sum_\lambda \max[\alpha_\lambda (c_0 + \eta_\lambda \vec{c} \cdot \hat{n}_\lambda), 0] - \sum_\lambda \alpha_\lambda c_0 - \sum_\lambda \alpha_\lambda \eta_\lambda \vec{c} \cdot \hat{n}_\lambda \\ &= \sum_\lambda |\alpha_\lambda (c_0 + \eta_\lambda \vec{c} \cdot \hat{n}_\lambda)|, \end{aligned} \quad (39)$$

where we use  $\sum_\lambda \alpha_\lambda = 1$  and  $\sum_\lambda \alpha_\lambda \eta_\lambda \hat{n}_\lambda = \vec{0}$  in the first equality.

When varying over all choices of operator  $C$  (thus, all inequalities that bound the convex set  $\mathcal{M}_{\{\Pi_\lambda\}}$ ), we finally arrive at the criteria:

$$|\vec{n}| \leq \frac{\inf_{c_0, \vec{c}} \sum_\lambda |\alpha_\lambda (c_0 + \eta_\lambda \vec{c} \cdot \hat{n}_\lambda)|}{|\vec{c}|}. \quad (40)$$

Since we are always allowed to scale  $c_0$  and  $|\vec{c}|$ , the above infimum can be further simplified with constraint  $|\vec{c}| = 1$  and  $-1 \leq c_0 \leq 1$ :

$$R(\{\Pi_\lambda\}) = \inf_{\substack{|\vec{c}|=1 \\ -1 \leq c_0 \leq 1}} \sum_\lambda |\alpha_\lambda(c_0 + \eta_\lambda \vec{c} \cdot \hat{n}_\lambda)| \quad (41)$$

The compatibility radius  $R(n)$  can then be expressed as

$$R(n) = \sup_{\{\Pi_\lambda\}} \inf_{\substack{|\vec{c}|=1 \\ -1 \leq c_0 \leq 1}} \sum_\lambda |\alpha_\lambda(c_0 + \eta_\lambda \vec{c} \cdot \hat{n}_\lambda)|, \quad (42)$$

where the superior is taken over all  $n$ -element POVMs.  $\square$

**Corollary 4.**  $R(n)$  is maximized by rank-1 POVM  $\{\Pi_n\}$ , i.e.,  $\eta_\lambda = 1$  for  $i \in [n]$ .

*Proof.* Given any POVM  $\{\Pi_n\}$  with  $\Pi_\lambda = \alpha_\lambda(\mathbb{I} + \eta_\lambda \hat{n}_\lambda \cdot \vec{\sigma})$ , we can define POVM  $\{\Pi'_i\}$  with:

$$\Pi'_i = \beta_i(\mathbb{I} + \hat{n}_\lambda \cdot \vec{\sigma})$$

where  $\beta_i = \frac{\alpha_\lambda \eta_\lambda}{\sum_j \alpha_j \eta_j}$ . Let  $c_0^*$  and  $\vec{c}^*$  be such that

$$R(\{\Pi'_\lambda\}) = \inf_{\substack{|\vec{c}|=1 \\ -1 \leq c_0 \leq 1}} \sum_\lambda |\beta_i(c_0 + \vec{c} \cdot \hat{n}_\lambda)| = \sum_\lambda |\beta_i(c_0^* + \vec{c}^* \cdot \hat{n}_\lambda)| = \frac{1}{\sum_j \alpha_j \eta_j} \sum_\lambda |\alpha_\lambda \eta_\lambda(c_0^* + \vec{c}^* \cdot \hat{n}_\lambda)|$$

For each individual term above,

$$|\alpha_\lambda \eta_\lambda(c_0^* + \vec{c}^* \cdot \hat{n}_\lambda)| + |(1 - \eta_\lambda) \alpha_\lambda c_0^*| \geq |\alpha_\lambda(c_0^* + \eta_\lambda \vec{c}^* \cdot \hat{n}_\lambda)|.$$

Summing over  $i$ , we have

$$\sum_\lambda |\alpha_\lambda \eta_\lambda(c_0^* + \vec{c}^* \cdot \hat{n}_\lambda)| + \sum_\lambda |(1 - \eta_\lambda) \alpha_\lambda c_0^*| \geq \sum_\lambda |\alpha_\lambda(c_0^* + \eta_\lambda \vec{c}^* \cdot \hat{n}_\lambda)|,$$

which is equivalent to

$$\sum_j \alpha_j \eta_j R(\{\Pi'_\lambda\}) + (1 - \sum_j \alpha_j \eta_j) |c_0^*| \geq \sum_\lambda |\alpha_\lambda(c_0^* + \eta_\lambda \vec{c}^* \cdot \hat{n}_\lambda)| \geq R(\{\Pi_\lambda\}).$$

The last inequality holds because  $(c_0^*, \vec{c}^*)$  might not be the optimal choice for  $\{\Pi_\lambda\}$ .

The last piece of the proof relies on showing  $R(\{\Pi'_\lambda\}) \geq |c_0^*|$ . This holds because:

$$R(\{\Pi'_\lambda\}) = \sum_\lambda |\beta_i(c_0^* + \vec{c}^* \cdot \hat{n}_\lambda)| \geq |\sum_\lambda \beta_i(c_0^* + \vec{c}^* \cdot \hat{n}_\lambda)| = |c_0^*|$$

Therefore, we finally have:

$$R(\{\Pi'_\lambda\}) \geq R(\{\Pi_\lambda\}).$$

$\square$

**Remark.** For symmetric POVM  $\text{sym}\{\Pi_\lambda\}$ , the compatible radius can be computed as

$$R(\text{sym}\{\Pi_\lambda\}) = \min_{\hat{c}} \sum_{i=1}^n \alpha_\lambda |(\hat{c} \cdot \hat{n}_\lambda)| \quad (43)$$

To show this is true for all symmetrically symmetric POVM, notice that optimization  $\inf_x (|x+y| + |x-y|)$  is always obtained with  $x = 0$ , thus

$$R(\text{sym}\{\Pi_\lambda\}) = \inf_{\substack{|\vec{c}|=1 \\ -1 \leq c_0 \leq 1}} \frac{1}{2} [\sum_\lambda |\alpha_\lambda(c_0 + \eta_\lambda \vec{c} \cdot \hat{n}_\lambda)| + \sum_\lambda |\alpha_\lambda(c_0 - \eta_\lambda \vec{c} \cdot \hat{n}_\lambda)|] = \min_{\hat{c}} \sum_{i=1}^n \alpha_\lambda |(\hat{c} \cdot \hat{n}_\lambda)| \quad (44)$$

**Corollary 5.** The Compatible radius  $R(\{\Pi_\lambda\})$  can be computed by considering a finite set of operators  $C = c_0 \mathbb{I} + \vec{c} \cdot \vec{\sigma}$ , where  $(c_0, \vec{c})^T$  is defined by the norm vector of facets of  $\mathfrak{M}_{\{\Pi_\lambda\}}$ .

*Proof.* As discussed in Section A, the compatible region is a convex zonotope. Instead of running over all hyperplane boundaries given by operator  $C = c_0\mathbb{I} + \vec{c} \cdot \vec{\sigma}$ , it suffices to consider a finite set of the operator  $C$  that define the normal vectors of those facets. A similar idea has been brought up in [16].

From the property of a zonotope, every edge of the compatible region  $\mathfrak{M}_{\{\Pi_\lambda\}}$  is always parallel to one of its generator vectors  $(1, \hat{n}_\lambda)$ , while each facet is defined by  $d - 1 = 3$  edges of the set. Therefore, we just have to consider at most  $\binom{n}{3}$  different choices of normal vectors. To be more specific, the vector  $(c_0, \vec{c})$  should be perpendicular to three different vectors  $(1, \hat{n}_\lambda)$ . Hence, we can write

$$\vec{c} = \frac{(\hat{n}_x - \hat{n}_y) \times (\hat{n}_x - \hat{n}_z)}{|(\hat{n}_x - \hat{n}_y) \times (\hat{n}_x - \hat{n}_z)|}, \quad c_0 = -\vec{c} \cdot \hat{n}_x \quad (45)$$

where  $\hat{n}_x, \hat{n}_y$  and  $\hat{n}_z$  are any choices of distinct vectors associated to POVM  $\{\Pi_\lambda\}$ . Therefore, we can now simplify the criteria above by calculating the minimum value over a finite set of size  $\binom{n}{3}$ .

Similarly, for the case with planar measurement, the vector  $(c_0, \vec{c})$  should be perpendicular to two different vectors  $(1, \hat{n}_\lambda)^T$ . Hence we can write:

$$(c_0, \vec{c})^T = (1, \hat{n}_x)^T \times (1, \hat{n}_y)^T \quad (46)$$

where  $\vec{c}, \hat{n}_\lambda$  are written as vectors in  $\mathbb{R}^2$ .  $\square$

## E Example of $R(\{\Pi_\lambda\})$ for symmetric POVMs, and compatible models

In this section, we compute the compatible radius  $R(\{\Pi_\lambda\})$  for different classes of symmetric POVMs, including:

**Result 1:** the compatible radius for rotationally symmetric planar measurements;

**Result 2:** a compatible model for rotationally symmetric planar measurements;

**Result 3:** the compatible radius for POVMs with regular polyhedron configuration.

**Result 1.** For equally spaced planar measurement  $\{\Pi_\lambda^{\text{rot}} = \frac{1}{n}(\mathbb{I} + \hat{n}_\lambda \cdot \sigma)\}$  with  $\hat{n}_\lambda = [\cos(\frac{2\pi\lambda}{n}), 0, \sin(\frac{2\pi\lambda}{n})]^T$ , we have:

$$R^p(\{\Pi_\lambda^{\text{rot}}\}) = \begin{cases} \frac{1}{n} \cot(\frac{\pi}{2n}) \cos(\frac{\pi}{2n}) & \text{if } n \text{ is odd} \\ \frac{2}{n} \cot(\frac{\pi}{n}) & \text{if } n \text{ is even.} \end{cases} \quad (47)$$

*Proof.* If  $n$  is even, the original vectors  $\hat{n}_\lambda$  form a regular polygon with  $n$  sides. To get the extreme point  $M_i^n \in \mathcal{M}_{\{\Pi_\lambda\}}$ , we can simply add up half of  $\{\Pi_\lambda^{\text{rot}}\}$  and obtain:

$$M_i^n = \sum_{j=i}^{j=n/2+i-1} \Pi_j^{\text{rot}} = \frac{1}{2}(\mathbb{I} + \vec{m}_i \cdot \sigma) \quad (48)$$

where  $\{\vec{m}_i\}$  form exactly the same regular polygon with  $|\vec{m}_i| = \frac{2}{n \sin(\frac{\pi}{n})}$ .

Given an  $n$ -sided regular polygon, the ratio between its inscribed radius and circumscribed radius is  $\frac{r_i}{r_c} = \cos(\frac{\pi}{n})$ . Therefore, the circle contained in the  $n$ -sided polygon defined by  $\vec{m}_i$  has radius

$$r_n = \frac{r_i}{r_c} |\vec{m}_i| = \cos(\frac{\pi}{n}) \cdot \frac{2}{n \sin(\frac{\pi}{n})} = \frac{2}{n} \cot(\frac{\pi}{n}). \quad (49)$$

If  $n$  is odd, the case is slightly different; instead, the extreme points can be enumerated as

$$\begin{aligned} M_i^n &= \sum_{j=i}^{j=(n-1)/2+i-1} \Pi_j^{\text{rot}} + \frac{1}{2} \Pi_{(n+1)/2+i-1}^{\text{rot}} = \frac{1}{2}(\mathbb{I} + \vec{m}_i \cdot \sigma) \\ W_i^n &= \sum_{j=i}^{j=(n-1)/2+i-1} \Pi_j^{\text{rot}} + \frac{1}{2} \Pi_{i-1}^{\text{rot}} = \frac{1}{2}(\mathbb{I} + \vec{w}_i \cdot \vec{\sigma}). \end{aligned} \quad (50)$$

In total there are  $2n$  vectors  $\{\vec{m}_i\} \cup \{\vec{w}_i\}$  which forms a  $2n$ -sided regular polygon with  $|\vec{m}_i| = |\vec{w}_i| = \frac{1}{n} \cot(\frac{\pi}{2n})$  and radius

$$r_n = \frac{r_i}{r_c} |\vec{m}_i| = \cos(\frac{\pi}{2n}) \cdot \frac{1}{n} \cot(\frac{\pi}{2n}) = \frac{1}{n} \cot(\frac{\pi}{2n}) \cos(\frac{\pi}{2n}). \quad (51)$$

$\square$

From our Table I in the main text, we observe that when  $n$  is odd, the rotationally symmetric scheme appears to be optimal. However, for even  $n$ , it is consistently suboptimal. This can be quantitatively explained by the fact that the unbiased compatible region  $\mathbf{m}_{\{\Pi_\lambda\}}$  is an  $n$ -sided polygon for even  $n$ , but a  $2n$ -sided polygon for odd  $n$ . More specifically, when  $n$  is even, there is an inherent trade-off between maximizing the number of sides of  $\mathbf{m}_{\{\Pi_\lambda\}}$  and maintaining its symmetry. The rotationally symmetric scheme exhibits the highest degree of symmetry; however, in this case, the unbiased compatible region has only  $n$  sides. In contrast, by adopting a slightly asymmetric POVM, we can construct a  $2n$ -sided  $\mathbf{m}_{\{\Pi_\lambda\}}$ , which, while not a regular polygon, results in a larger inradius.

**Corollary 6.** For any  $r \in [0, \frac{2}{\pi}]$ ,

$$\gamma^p(\omega_r) = N^p(r) \leq \sqrt{\frac{5\pi}{12}} \left( \frac{2}{\pi} - r \right)^{-1/2} + 1. \quad (52)$$

The extra  $+1$  term comes from the fact that for  $n$ -outcome planar POVMs with even  $n$ , we trivially apply the optimal scheme with an  $(n+1)$ -outcome measurement.

**Result 2.** Here we give the compatible model (equivalently a local hidden state model) when the parent POVM is rotationally symmetric.

For finite  $n$ , with parent POVM  $\Pi_\lambda^{\text{rot}} = \frac{1}{n}(\mathbb{I} + \hat{n}_\lambda \cdot \vec{\sigma})$ , any arbitrary child POVM  $T = \frac{1}{2}(\mathbb{I} + R(\{\Pi_\lambda^{\text{rot}}\})\hat{t} \cdot \vec{\sigma})$  with  $\hat{t} = (\cos(\theta), 0, \sin(\theta))^T$  can be simulated as

$$T = \sum_{\lambda} p_{\lambda} \Pi_{\lambda}^{\text{rot}}$$

For even  $n$ :

$$p_{\lambda} = \frac{1 + \frac{\text{sign}(\hat{m}_1 \cdot \hat{n}_\lambda) \sin(\frac{\pi}{n} - x) + \text{sign}(\hat{m}_2 \cdot \hat{n}_\lambda) \sin(\frac{\pi}{n} + x)}{2 \sin(\frac{\pi}{n})}}{2}$$

with  $x = \theta + \frac{2\pi k}{n} \in [-\frac{\pi}{n}, \frac{\pi}{n}]$ ,  $\hat{m}_1 = [\cos(\frac{2\pi(k-\frac{1}{2})}{n}), 0, \sin(\frac{2\pi(k-\frac{1}{2})}{n})]^T$ ,  $\hat{m}_2 = [\cos(\frac{2\pi(k+\frac{1}{2})}{n}), 0, \sin(\frac{2\pi(k+\frac{1}{2})}{n})]^T$  and  $k \in \mathbb{Z}$ .

For odd  $n$ :

$$p_{\lambda} = \frac{1 + \frac{\text{sign}(\hat{m}_1 \cdot \hat{n}_\lambda) \sin(\frac{\pi}{2n} - x) + \text{sign}(\hat{m}_2 \cdot \hat{n}_\lambda) \sin(\frac{\pi}{2n} + x)}{2 \sin(\frac{\pi}{2n})}}{2}$$

with  $x = \theta + \frac{\pi k}{n} \in [-\frac{\pi}{2n}, \frac{\pi}{2n}]$ ,  $\hat{m}_1 = [\cos(\frac{\pi(k-\frac{1}{2})}{n}), 0, \sin(\frac{\pi(k-\frac{1}{2})}{n})]^T$ ,  $\hat{m}_2 = [\cos(\frac{\pi(k+\frac{1}{2})}{n}), 0, \sin(\frac{\pi(k+\frac{1}{2})}{n})]^T$  and  $k \in \mathbb{Z}$ .

When taking  $n \rightarrow \infty$ , we have  $\hat{m}_1 = \hat{m}_2 = \hat{t}_i$  and  $\sin(f(x)) \rightarrow f(x)$  when  $f(x) \rightarrow 0$ . The above model becomes:

$$p_{\lambda} = \frac{1 + \frac{\text{sign}(\hat{m}_1 \cdot \hat{n}_\lambda) \sin(\frac{\pi}{n} - x) + \text{sign}(\hat{m}_2 \cdot \hat{n}_\lambda) \sin(\frac{\pi}{n} + x)}{2 \sin(\frac{\pi}{n})}}{2} \rightarrow \frac{1 + \frac{\text{sign}(\hat{t} \cdot \hat{n}_\lambda)(\frac{2\pi}{n} - x) + \text{sign}(\hat{t} \cdot \hat{n}_\lambda)x}{2 \frac{2\pi}{n}}}{2} = \frac{1 + \text{sign}(\hat{t} \cdot \hat{n}_\lambda)}{2} \quad (53)$$

Letting  $\lim_{n \rightarrow \infty} \sum_{i=1}^n (\cdot) \frac{1}{n} = \int_0^{2\pi} (\cdot) \frac{d\psi}{2\pi}$ , we can define  $\Pi_{\psi} = \frac{1}{2\pi}(\mathbb{I} + \hat{n}_{\psi} \cdot \vec{\sigma})$  and  $p_{\psi} = \frac{1 + \text{sign}(\hat{t} \cdot \hat{n}_{\psi})}{2}$  from the discrete one above to a continuous one, where  $\hat{n}_{\psi} = (\cos(\psi), 0, \sin(\psi))^T$ . Therefore, any child POVM  $T = \frac{1}{2}(\mathbb{I} + \frac{2}{\pi} \hat{t} \cdot \vec{\sigma})$  can be written as:

$$T = \int_0^{2\pi} d\theta p_{\psi} \Pi_{\psi} = \int_0^{2\pi} d\psi \left( \frac{1 + \text{sign}(\hat{t} \cdot \hat{n}_{\psi})}{2} \right) \frac{1}{2\pi} (\mathbb{I} + \hat{n}_{\psi} \cdot \vec{\sigma}) = \frac{1}{2} (\mathbb{I} + \frac{2}{\pi} \hat{t} \cdot \vec{\sigma}) \quad (54)$$

**Result 3.** For a parent POVM  $\{\Pi_{\lambda}\}$  with platonic-solid configuration, we can compute the  $R(\{\Pi_{\lambda}\})$  similarly using Result 1. The polyhedron  $\mathcal{M}_{\{\Pi_{\lambda}\}}$  associated with different platonic configurations are summarized below:

Complexity	POVM $\{\Pi_\lambda\}$	Compatible region $\mathbf{m}_{\{\Pi_\lambda\}}$	compatible radius $\mathcal{R}(\{\Pi_\lambda\})$
4	tetrahedron	Octahedron	$\frac{1}{3}$
6	Octahedron	Cube	$\frac{1}{3}$
8	Cube	Rhombic dodecahedron	$\frac{\sqrt{6}}{6}$
12	Icosahedron	Rhombic triacontahedron	$\frac{\phi^3 \sqrt{1+(1-\phi)^2}}{3(1+\phi^2)}$
20	Dodecahedron	Rhombic enneacanthahedron	$\sqrt{\frac{5}{6}} \frac{\phi^2}{5}$

Table 5: Parent POVM with platonic configuration and their associated unbiased compatible region  $\mathbf{m}_{\{\Pi_\lambda\}}$ , where  $\phi = \frac{1+\sqrt{5}}{2}$  is the golden ratio.

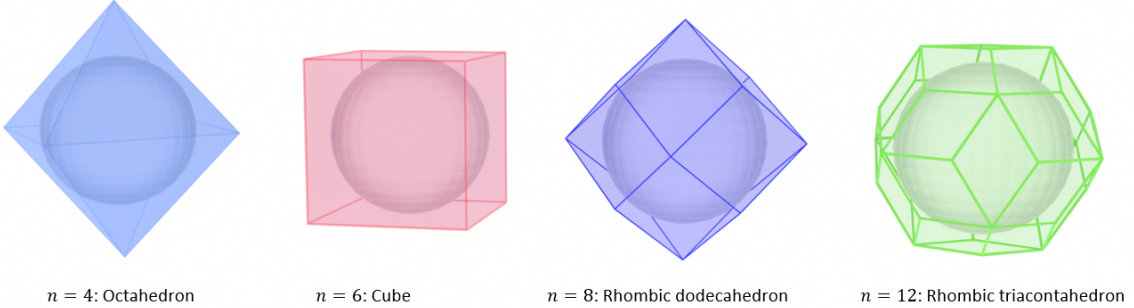


Figure 3: Compatible region for Platonic solid with  $n = 4, 6, 8, 12$ . From left to right: Octahedron, Cube, Rhombic dodecahedron and Rhombic triacontahedron .

**Tetrahedron:** With the vertices of an Tetrahedron, we can construct a 4-element parent POVM as follows:

$$\Pi_\lambda^T = \frac{1}{4}(\mathbb{I} + \hat{n}_\lambda \cdot \vec{\sigma}) \quad \text{with } \hat{n}_\lambda \in \left\{ \frac{1}{\sqrt{3}}(1, 1, 1), \frac{1}{\sqrt{3}}(1, -1, -1), \frac{1}{\sqrt{3}}(-1, 1, -1), \frac{1}{\sqrt{3}}(-1, -1, 1) \right\} \quad (55)$$

The extreme points of the associated compatible region  $\mathbf{m}_{\{\Pi_\lambda\}}$  can be computed as:

$$M_\lambda^T = \frac{1}{2}(\mathbb{I} + \vec{m}_\lambda \cdot \vec{\sigma}) \quad \text{with } \vec{m}_\lambda \in \left\{ \frac{1}{\sqrt{3}}(\pm 1, 0, 0), \frac{1}{\sqrt{3}}(0, \pm 1, 0), \frac{1}{\sqrt{3}}(0, 0, \pm 1) \right\} \quad (56)$$

These 6 vertices altogether form a convex polyhedron – Octahedron, to calculate the inscribed radius, we have:

$$r^T = |\vec{m}_\lambda| \cdot \frac{1}{\sqrt{3}} = \frac{1}{3}$$

**Octahedron:** With the vertices of a Tetrahedron, we can construct a 6-element parent POVM as follows:

$$\Pi_\lambda^O = \frac{1}{6}(\mathbb{I} + \hat{n}_\lambda \cdot \vec{\sigma}) \quad \vec{n}_\lambda \in \{(\pm 1, 0, 0), (0, \pm 1, 0), (0, 0, \pm 1)\}, \quad (57)$$

The extreme points of the associate compatible region  $\mathbf{m}_{\{\Pi_\lambda^O\}}$  can be computed as:

$$M_\lambda^O = \frac{1}{2}(\mathbb{I} + \vec{m}_\lambda \cdot \vec{\sigma}) \quad \vec{m}_\lambda \in \left\{ \frac{1}{3}(\pm 1, \pm 1, \pm 1) \right\}, \quad (58)$$

These 8 vertices altogether form a convex polyhedron – Cube, to calculate the inscribed radius, we have:

$$r^O = |\vec{m}_\lambda| \cdot \frac{1}{\sqrt{3}} = \frac{1}{3}$$

**Cube:** With the vertices of a Tetrahedron, we can construct an 8-element parent POVM as follows:

$$\Pi_\lambda^C = \frac{1}{8}(\mathbb{I} + \hat{n}_\lambda \cdot \vec{\sigma}) \quad \vec{n}_\lambda \in \left\{ \frac{1}{\sqrt{3}}(\pm 1, \pm 1, \pm 1) \right\} \quad (59)$$

The extreme point of the associate compatible region  $\mathbf{m}_{\{\Pi_\lambda^C\}}$  can be computed as:

$$M_\lambda^C = \frac{1}{2}(\mathbb{I} + \vec{m}_\lambda \cdot \vec{\sigma}) \quad \text{with } \vec{m}_\lambda \in \left\{ \frac{1}{2\sqrt{3}}(\pm 1, \pm 1, \pm 1), \frac{1}{2\sqrt{3}}(\pm 2, 0, 0), \frac{1}{2\sqrt{3}}(0, \pm 2, 0), \frac{1}{2\sqrt{3}}(0, 0, \pm 2) \right\} \quad (60)$$

These 14 vertices altogether form a convex polyhedron – Rhombic dodecahedron with edge length  $a = |\vec{m}_\lambda - \vec{m}_j| = \frac{1}{2}$

$$r^C = \frac{\sqrt{6}}{3} \cdot \frac{1}{2} = \frac{\sqrt{6}}{6} \approx 0.408$$

**Icosahedron:** With the vertices of an icosahedron, we can construct a 12-element parent POVM as following:

$$\Pi_\lambda^I = \frac{1}{12}(\mathbb{I} + \hat{n}_\lambda \cdot \vec{\sigma}) \quad \text{with } \hat{n}_\lambda \in \left\{ \frac{1}{\sqrt{1+\phi^2}}(0, \pm 1, \pm \phi), \frac{1}{\sqrt{1+\phi^2}}(\pm \phi, 0, \pm 1), \frac{1}{\sqrt{1+\phi^2}}(\pm 1, \pm \phi, 0) \right\} \quad (61)$$

where  $\phi = \frac{1+\sqrt{5}}{2}$ . This time the extreme points of the associate compatible region  $\mathbf{m}_{\{\Pi_\lambda\}}$  can be computed as:

$$\begin{aligned} M_\lambda^I = \frac{1}{2}(\mathbb{I} + \hat{m}_\lambda \cdot \vec{\sigma}) \quad \text{with } \hat{m}_i \in & \left\{ \frac{\phi}{3\sqrt{1+\phi^2}}(0, \pm 1, \pm \phi), \frac{\phi}{3\sqrt{1+\phi^2}}(\pm \phi, 0, \pm 1), \frac{\phi}{3\sqrt{1+\phi^2}}(\pm 1, \pm \phi, 0) \right\} \\ \cup & \left\{ \frac{\phi}{3\sqrt{1+\phi^2}}(\pm 1, \pm 1, \pm 1), \frac{\phi}{3\sqrt{1+\phi^2}}(0, \pm \phi, \pm 1/\phi), \frac{\phi}{3\sqrt{1+\phi^2}}(\pm 1/\phi, 0, \pm \phi), \frac{\phi}{3\sqrt{1+\phi^2}}(\pm \phi, \pm 1/\phi, 0) \right\} \end{aligned} \quad (62)$$

These 32 vertices altogether form a convex polyhedron – Rhombic triacontahedron, to calculate the inscribed radius, we first notice that the edge length of Rhombic triacontahedron given as  $a = |\vec{m}_\lambda - \vec{m}_j| = \frac{\phi}{3\sqrt{1+\phi^2}}\sqrt{1+(1-\phi)^2}$ , and the inscribed radius is  $r = \frac{\phi^2}{\sqrt{1+\phi^2}}a$ . Therefore, the radius of the shrinking Bloch sphere built by parent POVM  $\{\Pi_i^I\}$  will be

$$r^I = \frac{\phi}{3\sqrt{1+\phi^2}}\sqrt{1+(1-\phi)^2} \cdot \frac{\phi^2}{\sqrt{1+\phi^2}} \approx 0.4588$$

**Dodecahedron:** With the vertices of a dodecahedron, we can construct a 20-element parent POVM as follows:

$$\begin{aligned} \Pi_\lambda^D = \frac{1}{20}(\mathbb{I} + \hat{n}_\lambda \cdot \vec{\sigma}) \quad \text{with } \hat{n}_\lambda \in & \left\{ \frac{1}{\sqrt{3}}(\pm 1, \pm 1, \pm 1) \right\} \\ \text{or with } \hat{n}_\lambda \in & \left\{ \frac{1}{\sqrt{1+\phi^4}}(0, \pm 1, \pm \phi^2), \frac{1}{\sqrt{1+\phi^4}}(\pm \phi^2, 0, \pm 1), \frac{1}{\sqrt{1+\phi^4}}(\pm 1, \pm \phi^2, 0) \right\} \end{aligned} \quad (63)$$

The extreme points of the associate compatible region  $\mathbf{m}_{\{\Pi_\lambda^D\}}$  can be computed as:

$$\begin{aligned} M_\lambda^D = \frac{1}{2}(\mathbb{I} + \hat{m}_\lambda \cdot \vec{\sigma}) \quad \text{with } \hat{m}_i \in & \left\{ \frac{2(\phi^2+1)}{10\sqrt{3}\phi}(0, \pm \phi, \pm 1), \frac{2(\phi^2+1)}{10\sqrt{3}\phi}(\pm \phi, \pm 1, 0), \frac{2(\phi^2+1)}{10\sqrt{3}\phi}(0 \pm 1, 0, \pm \phi) \right\} \\ \cup & \left\{ \frac{2\phi^2}{10\sqrt{3}}(\pm 1, \pm 1, \pm 1), \frac{2\phi^2}{10\sqrt{3}}(0, \pm 1/\phi, \pm \phi), \frac{2\phi^2}{10\sqrt{3}}(\pm \phi, 0, \pm 1/\phi), \frac{2\phi^2}{10\sqrt{3}}(\pm 1/\phi, \pm \phi, 0) \right\} \\ \cup & \left\{ \frac{2\phi^2}{10\sqrt{3}}(\pm 2/\phi, \pm 1/\phi^2, \pm 1), \frac{2\phi^2}{10\sqrt{3}}(\pm 1/\phi^2, \pm 1, \pm 2/\phi), \frac{2\phi^2}{10\sqrt{3}}(\pm 1, \pm 2/\phi, \pm 1/\phi^2) \right\} \\ \cup & \left\{ \frac{2\phi^2}{10\sqrt{3}}(\pm \phi, \pm 1/\phi, \pm 1/\phi), \frac{2\phi^2}{10\sqrt{3}}(\pm 1/\phi, \pm \phi, \pm 1/\phi), \frac{2\phi^2}{10\sqrt{3}}(\pm 1/\phi, \pm 1/\phi, \pm \phi) \right\} \\ \cup & \left\{ \frac{1}{10\sqrt{3}}(\pm 2(\phi^2+1), \pm 2(\phi-1), 0), \frac{1}{10\sqrt{3}}(\pm 2(\phi-1), \pm 2(\phi^2+1), 0), \frac{1}{10\sqrt{3}}(0, \pm 2(\phi^2+1), \pm 2(\phi-1)) \right\} \end{aligned} \quad (64)$$

These 92 vertices altogether form a convex polyhedron – Rhombic enneacontahedron, the inradius of which can be computed as:

$$r^D = \sqrt{\frac{5}{6}} \frac{\phi^2}{5} = 0.4780$$

## F Simulation cost of entangled state and compatible measurements

**Lemma 1.**  $\mathcal{P}_r$  can be simulated with an  $n$ -element POVM if and only if the simulation cost of Werner state  $\omega_r$  under *projective measurements* equals  $n$ .

*Proof.* Consider the case where  $M_{a|x}$  can be simulated with a  $n$ -element parent POVM  $\Pi_\lambda$  by  $M_{a|x} = \sum_\lambda p(a|x, \lambda) \Pi_\lambda$ , then any assemblage  $\{\sigma_{a|x}\}$  can be written as:

$$\sigma_{a|x} = \text{Tr}_A[(M_{a|x} \otimes \mathbb{I})\rho_{AB}] = \sum_\lambda p(a|x, \lambda) \text{Tr}_A[(\Pi_\lambda \otimes \mathbb{I})\rho_{AB}] \quad (65)$$

Let  $\sigma_\lambda = \text{Tr}_A[(\Pi_\lambda \otimes \mathbb{I})\rho_{AB}]$ , this becomes a LHS model for assemblage  $\{\sigma_{a|x}\}$ , which has complexity  $n$  and thus requiring  $\log_2 n$  bits shared randomness.

Conversely, we consider state assembly prepared by  $\rho_{AB} = |\Phi^+\rangle\langle\Phi^+|$  with  $|\Phi^+\rangle = \frac{1}{\sqrt{2}}(|00\rangle + |11\rangle)$ , we have

$$\sigma_{a|x} = \text{Tr}_A[(M_{a|x} \otimes \mathbb{I})|\Phi^+\rangle\langle\Phi^+|] = \frac{1}{2} M_{a|x}^T \quad (66)$$

If assemblage  $\{\sigma_{a|x}\}$  has a LHS model  $\sigma_{a|x} = \sum_\lambda p(a|x, \lambda) \sigma_\lambda$  with  $\log_2 n$  bit shared randomness, we can find a compatible model for the set of measurements  $\{M_{a|x}\}$  as:

$$M_{a|x} = \sum_\lambda p(a|x, \lambda) 2\sigma_\lambda^T, \quad (67)$$

Where we could define  $\Pi_\lambda = 2\sigma_\lambda^T$  (note that  $\sum_a \sigma_{a|x} = \sum_a \sum_\lambda p(a|x, \lambda) \sigma_\lambda = \sum_\lambda \sigma_\lambda = \frac{\mathbb{I}}{2}$ ). Hence, the set of measurements  $M_{a|x}$  can be simulated with  $\log_2 n$  shared randomness, or  $n$ -outcome POVM  $\{\Pi_\lambda\}$ .

Since qubit Werner state is only different from  $|\Phi^+\rangle\langle\Phi^+|$  by a local unitary transformation, i.e.,  $\rho_W = U_y \otimes U_y |\Phi^+\rangle\langle\Phi^+| U_y \otimes U_y$ , where  $U_y$  stands for Pauli operator. If assemblage  $\{\sigma_{a|x}\}$  has a LHS model  $\sigma_{a|x} = \sum_\lambda p(a|x, \lambda) \sigma_\lambda$  with  $\log_2 n$  bit shared randomness, we can find a compatible model for the set of measurements  $\{M_{a|x}\}$  as:

$$M_{a|x} = \sum_\lambda p(a|x, \lambda) 2[U_y \sigma_\lambda U_y]^T. \quad (68)$$

Therefore, we conclude that the problem of building LHS models for the Werner state using finite SR can be mapped one-to-one to a compatible radius problem.  $\square$

## G Discussion on prop. 1, prop. 2 and conj. 1

### 1 Inequivalence between simulation cost of PVMs and POVMs

In an earlier paper[33], we demonstrated the equivalence of POVMs and PVMs in the context of quantum steering. We achieve this by establishing that a compatible model exists for all noisy POVMs whenever such a model exists for all noisy PVMs at the same noise threshold. However, this elegant equivalence disappears when considering scenarios that involve only finite-shared randomness and specific parent POVMs (or specific local hidden states).

In the main text, we conduct an extensive discussion on the feasibility of a compatible model for noisy PVMs with finite shared randomness. Notably, one intriguing observation we make there is that the optimal parent POVM for simulating the entire set of noisy PVMs may not necessarily be centrally symmetric, even if it does exist. The realization that asymmetry has a role in simulating all PVMs provides insight into the potential divergence between POVMs and PVMs within this restricted compatible model.

In the following sections, we provide a rigorous proof for the aforementioned assertion using Farka's lemma. We want to show that a solution of  $A \cdot \mathbf{x} = \mathbf{b}$  exists with coefficients  $x_{a|i} \geq 0$  that also satisfy the condition  $\sum_a x_{a|i} = 1$  for all  $i = 1, \dots, n$  and  $a = 1, \dots, m$ , where

$$A = \begin{pmatrix} \vec{\pi}_1 & \cdots & \vec{\pi}_n & 0 & \cdots & 0 & 0 & 0 & 0 \\ \ddots & & & \ddots & & & \ddots & & \\ 0 & 0 & 0 & 0 & \cdots & 0 & \vec{\pi}_1 & \cdots & \vec{\pi}_n \\ 1 & \cdots & 0 & 1 & \cdots & 0 & 1 & \cdots & 0 \\ \ddots & & & \ddots & & & \ddots & & \\ 0 & \cdots & 1 & 0 & \cdots & 1 & 0 & \cdots & 1 \end{pmatrix}, \quad \mathbf{x} = \begin{pmatrix} x_{1|1} \\ \vdots \\ x_{1|n} \\ x_{2|n} \\ \vdots \\ x_{m|n} \end{pmatrix}, \quad \mathbf{b} = \begin{pmatrix} \vec{m}_1 \\ \vdots \\ \vec{m}_m \\ 1 \\ \vdots \\ 1 \end{pmatrix}. \quad (69)$$

**Lemma 2** (Farkas' Lemma).

$$\nexists \mathbf{x} \geq \mathbf{0} \text{ s.t. } A \cdot \mathbf{x} = \mathbf{b} \iff \exists \mathbf{y} \text{ s.t. } A^T \cdot \mathbf{y} \geq \mathbf{0} \text{ and } \mathbf{b}^T \cdot \mathbf{y} < 0 \quad (70)$$

where  $\mathbf{y} \in \mathbb{R}^{4m+n}$  as  $y = (\vec{y}_1, \dots, \vec{y}_m, z_1, \dots, z_n)^T$ .

Therefore, to demonstrate the non-existence of a positive, normalized response function  $x_{a|i}$  for simulating  $\{\tilde{M}_a\}$  with  $\{\Pi_\lambda\}_{\lambda=1}^n$ , it suffices to find a vector  $\mathbf{y}$  such that  $A^T \cdot \mathbf{y} \geq \mathbf{0}$  and  $\mathbf{b}^T \cdot \mathbf{y} < 0$  holds at the same time.

**Proposition 6.** There exists a five-effect parent POVM  $\{\Pi_\lambda\}_{\lambda=1}^5$  with  $R(\{\Pi_i\}) \approx 0.3714$ , that is, it can simulate all noisy spin measurements with radius  $r \leq 0.3714$ , whereas a compatible model fails to exist for some three-outcome noisy POVMs with radius  $r > 0.3220$

*Proof.* The 5-effect POVM  $\{\Pi_\lambda = \alpha_\lambda(\mathbb{I} + \hat{n}_\lambda \cdot \sigma)\}$  to be considered is of the form of:

$$\begin{aligned} \vec{\pi}_1 &= 0.242(1, \hat{n}_1)^T & \hat{n}_1 &= (1, 0, 0)^T \\ \vec{\pi}_2 &= 0.098(1, \hat{n}_2)^T & \hat{n}_2 &= (-1, 0, 0)^T \\ \vec{\pi}_3 &= 0.220(1, \hat{n}_3)^T & \hat{n}_3 &= \left(-\frac{12}{55}, \sqrt{1 - \left(\frac{12}{55}\right)^2}, 0\right)^T \\ \vec{\pi}_4 &= 0.220(1, \hat{n}_4)^T & \hat{n}_4 &= \left(-\frac{12}{55}, -\frac{1}{2}\sqrt{1 - \left(\frac{12}{55}\right)^2}, \frac{\sqrt{3}}{2}\sqrt{1 - \left(\frac{12}{55}\right)^2}\right)^T \\ \vec{\pi}_5 &= 0.220(1, \hat{n}_5)^T & \hat{n}_5 &= \left(-\frac{12}{55}, -\frac{1}{2}\sqrt{1 - \left(\frac{12}{55}\right)^2}, -\frac{\sqrt{3}}{2}\sqrt{1 - \left(\frac{12}{55}\right)^2}\right)^T \end{aligned} \quad (71)$$

First, we used the criteria for computing the compatible radius  $R(\{\Pi_\lambda\})$  in appendix D to obtain a close form expression:

$$R(\{\Pi_\lambda\}) = 0.34 + 0.144 \frac{12}{55} \approx 0.3714. \quad (72)$$

Therefore, any PVMs with visibility  $r \leq 0.3714$  can be simulated by the corresponding 5-outcome POVM.

Now, we give examples showing the infeasibility of simulating three-outcome POVMs  $\{M_a^r\}$  with this five-effect parent POVM for an even smaller threshold  $r < R(\{\Pi_\lambda\})$ . The specific three-outcome POVM  $\{M_a^r\}$  we consider is given by the four-vectors

$$\begin{aligned} \vec{m}_1 &= \frac{1}{3}(1, r\hat{m}_1)^T & \hat{m}_1 &= (0, -1, 0)^T \\ \vec{m}_2 &= \frac{1}{3}(1, r\hat{m}_2)^T & \hat{m}_2 &= (0, \frac{1}{2}, \frac{\sqrt{3}}{2})^T \\ \vec{m}_3 &= \frac{1}{3}(1, r\hat{m}_3)^T & \hat{m}_3 &= (0, \frac{1}{2}, -\frac{\sqrt{3}}{2})^T. \end{aligned} \quad (73)$$

By considering vector  $\mathbf{y} \in \mathbb{R}^{4 \times 3+5}$  as  $y = (\vec{y}_1, \vec{y}_2, \vec{y}_3, z_1, z_2, z_3, z_4, z_5)^T$ , where:

$$\begin{aligned} \vec{y}_1 &= (0, -\hat{m}_1)^T, & \vec{y}_2 &= (0, -\hat{m}_2)^T & \vec{y}_3 &= (0, -\hat{m}_3)^T \\ z_1 &= z_2 = z_3 = 0.110\sqrt{1 - \left(\frac{12}{55}\right)^2}, & z_4 &= z_5 & = 0, \end{aligned} \quad (74)$$

and  $A^T \cdot \mathbf{y} \geq 0$ , one can easily verify that with  $\mathbf{b} = (\vec{m}_1, \vec{m}_2, \vec{m}_3, 1, 1, 1, 1, 1)^T$ :

$$\mathbf{b}^T \cdot \mathbf{y} = -r + 0.330\sqrt{1 - \left(\frac{12}{55}\right)^2} < 0 \implies r > 0.330\sqrt{1 - \left(\frac{12}{55}\right)^2} \approx 0.3220 \quad (75)$$

Therefore, from Farka's lemma, for  $r > 0.3220$ , the three-outcome POVM defined in Eq. 73 can never be simulated by the five-effect POVM  $\{\Pi_\lambda\}$ , whereas all PVMs can be simulated by it with  $r < 0.3714$ .  $\square$

**Conjecture 1.** The 5-outcome POVM in Eq. 71 is near optimal in terms of simulating PVMs, i.e, close to the optimal  $\{\Pi_\lambda\}$  that has the largest compatible radius  $R(\{\Pi_\lambda\}) \approx 0.3718$  reported in the main text. Therefore, we conjecture that the set of noisy POVMs and noisy PVMs has different simulation costs.

## 2 Equivalence between simulation cost of PVMs and POVMs for qubit planar measurements

However, as noted in Proposition 2 in the main text, there exist special cases where the simulation cost of a set of noisy qubit PVMs and a set of noisy qubit POVMs is actually the same.

To continue our discussion, we define a few quantities generalized from the main text:

- (1)  $N_{\text{POVM}}^p(r)$ : the simulation cost of noisy planar qubit POVMs with a noise parameter  $r$ ;
- (2)  $R_{\text{POVM}}^p(n)$  the compatibility radius for simulating noisy planar qubit POVMs with  $n$ -outcome measurements.

The following lemma, which will be critical for the subsequent proposition, is stated and proved below:

**Lemma 3.**  $R_{\text{POVM}}^p(3) = R^p(3) = \frac{1}{2} \Leftrightarrow \gamma^p(\omega_{\frac{1}{2}}) = N^p(\frac{1}{2}) = 3$

*Proof.* We first notice that,  $R_{\text{POVM}}^p(3)$  has to be obtained by 3-outcome parent  $\{\Pi_i\}$  with linear independent effects since  $R^p(3) = 0$  otherwise.  $R_{\text{POVM}}^p(3) \leq R^p(3)$  is obvious since PVMs form a subset of POVMs.

To show  $R_{\text{POVM}}^p(3) \geq R^p(3)$ , for planar POVM  $\{M_a^r\}$ , it suffices to consider three outcome measurements since they are extreme in the planar case, given a fixed noise threshold  $r$ , if all noisy 3-outcome qubit planar measurement can be simulated, then all noisy qubit planar POVMs can be simulated. Each of its effects  $M_a^r$  can be simulated individually by  $\{\Pi_i\}$  for all  $r \leq R^p(3)$ , therefore there exist  $0 \leq p_{a|i} \leq 1$  such that  $M_a^r = \sum_{i=1}^3 p_{a|i} \Pi_i$ .

Now considering the two normalization condition:  $\sum_{a=1}^3 M_a^r = \sum_{i=1}^3 \Pi_i = \mathbb{I}$ , we have:

$$\sum_{i=1}^3 (1 - \sum_a p_{a|i}) \Pi_i = 0 \quad (76)$$

The linearly independence  $\Pi_i$  implies  $\sum_a p_{a|i} = 1$ , thus  $\{M_a^r\}_a$  can be simultaneous simulated by  $\{\Pi_i\}$ , and therefore,  $R_{\text{POVM}}^p(3) \geq R^p(3)$ . We thus have  $R_{\text{POVM}}^p(3) = R^p(3) = \frac{1}{2}$  which implies  $\gamma(\rho_W(\frac{1}{2})) = N^p(\frac{1}{2})$  using duality between compatibility of noisy spin measurements and steerability of Werner state as discussed in section F.  $\square$

Similarly one could show that

**Corollary 7.**  $R_{\text{POVM}}(4) = R(4) = \frac{1}{3} \Leftrightarrow \gamma(\rho_W(\rho_W(\frac{1}{3}))) = N(\frac{1}{3}) = 4$

**Proposition 7.**  $R_{\text{POVM}}^p(n) = R^p(n) \Leftrightarrow \gamma^p(\omega_r) = N^p(r)$ .

*Proof.* Assume POVM  $\{\Pi_i\}$  can simulate 2-outcome measurement  $\{M_a^r, \mathbb{I} - M_a^r\}$  with  $M_a^r = \sum_{i=1}^n p_{a|i} \Pi_i$ , we have

$$\sum_{i=1}^n \Pi_i = \sum_{a=1}^3 M_a^r = \mathbb{I} \implies (\sum_{a=1}^3 p_{a|i} - 1) \Pi_i = 0, \quad (77)$$

Thus, it is sufficient to show that there exists a set of coefficient  $p_{a|i}$  such that  $\sum_{a=1}^3 p_{a|i} = 1$  for all  $i$

**For  $n = 3$ :** As given in lem. 3, for linear independent  $\{\Pi_i\}_{i=1}^3$  we have  $\sum_a p_{a|i} = 1$

**For  $n = 4$ :** Since  $\sum_{a=1}^3 p_{a|i} = 1$  does not hold in general, we want to smooth  $p_{a|i}$  such that  $\sum_{a=1}^3 p_{a|i} = 1$

*Case 1:* If any of  $\sum_a p_{a|i} = 1$ , then the problem reduces to the case of  $n = 3$ . Thus  $\sum_{a=1}^3 p_{a|i} = 1$  for all  $i$ .

*Case 2:* If none of  $\sum_a p_{a|i} = 1$ , up to some index relabeling, their linear dependence is given as:

$$\begin{aligned} \sum_i q_i \Pi_i = 0 \quad \text{with} \quad q_i &:= \sum_a p_{a|i} - 1 > 0, \quad i = 1, 2 \\ q_i &:= \sum_a p_{a|i} - 1 < 0, \quad i = 3, 4 \end{aligned} \quad (78)$$

Since  $\sum_a p_{a|i} > 1$  for  $i = 1, 2$ , there must exist at least one  $a \in \{1, 2, 3\}$ , such that both elements  $p_{a|1} > 0$  and  $p_{a|2} > 0$ . And we can now construct  $M_a^r$  as

$$M_a^r = \sum_i p_{a|i} \Pi_i - \beta \sum_i q_i \Pi_i \implies \sum_i p'_{a|i} \Pi_i \quad (79)$$

For some  $\beta > 0$ , where the new  $p'_{a|i} = p_{a|i} - \beta q_i$  should still be a valid response function. When keep increasing  $\beta$  from 0, we might end up with two different sub-cases:

*case 2a:*  $\sum_a p_{a|i}$  becomes 1 for  $i = 1, 2$  (as they are decreasing). Then move to *case 1*.

case 2b:  $p_{a|i} = 0$  at first for  $i = 1, 2$  before  $\sum_a p_{a|i}$  reaching 1. Since in this case, we would still have  $q_i > 0$  for  $i = 1, 2$  while  $q_i < 0$  for  $i = 3, 4$ . There must exist  $a' \neq a$ , such that  $p_{a'|1} > 0$  and  $p_{a'|2} > 0$ . When then repeat case 2.

$$M_{a'}^r = \sum_i p_{a'|i} \Pi_i - \beta \sum_i q_i \Pi_i \implies \sum_i p_{a'|i} \Pi_i \quad (80)$$

Hence, in the end, we will always be able to construct a suitable  $p_{a|i}$  such that  $0 \leq p_{a|i} \leq 1$  and  $\sum_a p_{a|i} = 1$   
**For  $n \geq 5$ :** Assuming  $\sum_a p_{a|i} \neq 1$  for all  $i$ . We can divide these effects in two indexes set  $\mathcal{J}$  and  $\mathcal{K}$  based on the sign of  $q_i$ , and thus there must exist two pairs of  $\Pi_i$  such that

$$\sum_i q_i \Pi_i := t_{j_1} \Pi_{j_1}^p + t_{j_2} \Pi_{j_2}^p - t_{k_1} \Pi_{k_1}^p - t_{k_2} \Pi_{k_2}^p = 0$$

With this linear dependent relation, we can follow the same procedure as in  $n = 4$  iteratively and smooth  $\sum_a p_{a|i} = 1$  one by one until we get  $n = 3$   $\square$